

Review

Review of the State-of-the-Art Uses of Minimal Surfaces in Heat Transfer

Krzysztof Dutkowski ¹, Marcin Kruzel ^{1,*} and Krzysztof Rokosz ²

¹ Faculty of Mechanical Engineering, Koszalin University of Technology, Raclawicka Street 15-17, 75-620 Koszalin, Poland

² Faculty of Electronics and Computer Science, Koszalin University of Technology, Śniadeckich Street 2, 74-453 Koszalin, Poland

* Correspondence: marcin.kruzel@tu.koszalin.pl

Abstract: The design of heat exchangers may change dramatically through the use of additive manufacturing (AM). Additive manufacturing, colloquially known as 3D printing, enables the production of monolithic metal bodies, devoid of contact resistance. The small volume of the exchanger, its lightness of weight, and the reduction of its production costs, compared to conventional methods, make the production of heat exchangers by AM methods conventional technologies. The review study presents a new look at the TPMS as a promising type of developed surface that can be used in the area of heat transfer. (Thus far, the only attractive option. The most important feature of additive manufacturing is the ability to print the geometry of theoretically any topography. Such a topography can be a minimal surface or its extended version—triplly periodic minimal surface (TPMS). It was practically impossible to manufacture a TPMS-based heat exchanger with the method of producing a TPMS.) The issues related to the methods of additive manufacturing of metal products and the cycle of object preparation for printing were discussed, and the available publications presenting the results of CFD simulations and experimental tests of heat exchangers containing a TPMS in their construction were widely discussed. It has been noticed that the study of thermal-flow heat transfer with the use of TPMSs is a new area of research, and the number of publications in this field is very limited. The few data (mainly CFD simulations) show that the use of TPMSs causes, on the one hand, a several-fold increase in the number of Nu, and on the other hand, an increase in flow resistance. The use of TPMSs in heat exchangers can reduce their size by 60%. It is concluded that research should be carried out in order to optimize the size of the TPMS structure and its porosity so that the gains from the improved heat transfer compensate for the energy expenditure on the transport of the working fluid. It has been noticed that among the numerous types of TPMSs available for the construction of heat exchangers, practically, four types have been used thus far: primitive, gyroid, I-WP, and diamond. At the moment, the diamond structure seems to be the most promising in terms of its use in the construction of heat exchangers and heat sinks. It is required to conduct experimental research to verify the results of the CFD simulation.

Keywords: TPMS; additive manufacturing; 3D printing; minimal surface



Citation: Dutkowski, K.; Kruzel, M.; Rokosz, K. Review of the State-of-the-Art Uses of Minimal Surfaces in Heat Transfer. *Energies* **2022**, *15*, 7994. <https://doi.org/10.3390/en15217994>

Academic Editors: Sergio Nardini and Bernardo Buonomo

Received: 30 September 2022

Accepted: 24 October 2022

Published: 27 October 2022

Publisher's Note: MDPI stays neutral with regard to jurisdictional claims in published maps and institutional affiliations.



Copyright: © 2022 by the authors. Licensee MDPI, Basel, Switzerland. This article is an open access article distributed under the terms and conditions of the Creative Commons Attribution (CC BY) license (<https://creativecommons.org/licenses/by/4.0/>).

1. Introduction

One of the features of Industry 4.0 is the use of intelligent manufacturing technologies [1]. These include, but are not limited to, additive manufacturing (AM). Additive manufacturing enables the materialization of virtually any solid created using computer programs for 3D design. It was natural, then, that the engineering reached for shapes that were previously impossible or economically unjustified to manufacture. Some of these shapes are found in nature. One of them is the minimal surface. Its elementary form, duplicated in three directions, is the so-called triply periodic minimal surface (TPMS). TPMS structures have been discovered in the structure of a butterfly's wing or the scales of a weevil beetle [2].

Tests of TPMS structures obtained by AM technology show that thanks to the high surface to volume ratio [3–5], they are characterized by a low weight [6,7], a high stiffness [8–13], endurance [14–18], the ability to absorb energy [19–22], and a lack of edges which excludes places where mechanical stresses may arise [23–25].

The use of AM for the production of heat exchange devices seems to be a logical continuation of engineering research in terms of the possibility of using the TPMS. However, the use of many materials and alloys typical for the field of thermal engineering (e.g., pure copper [26]), encounters numerous barriers [27] in the manufacturing process with AM technologies. Overcoming them becomes a current challenge, as it is not difficult to imagine the advantages of a monolithic heat exchanger structure devoid of local thermal resistances hitherto existing in the place of various parts or materials that make up the heat exchanger.

At the moment, there are no articles in the literature containing a summary of information on the possibility of using TPMSs for the construction of heat exchangers and heat sinks; profits resulting from the use of TPMSs as one of the methods of intensifying heat transfer (expansion of the heat exchange surface); an increase in the energy expenditure needed to force the fluid to flow along the TPMS; the influence of various types of TPMSs on the obtained thermal and flow parameters of heat exchange devices; and operational tests of TPMS heat exchangers in the field of broadly understood low- and high-temperature thermal energy.

The paper presents a literature review on the use of AM for the production of heat transfer devices, and in particular, those based on the TPMS. The issues related to the additive manufacturing process, the applied AM techniques, the cycle that should be passed from the concept in the production phase through to AM, and the use of AM to the production of lattice structures were discussed. Another area of the described issues is the approximation of minimal surfaces as a representative of lattice structures, and TPMSs and the use of AM for the production of heat transfer devices, with particular emphasis on those devices that use a TPMS as a heat transfer surface.

2. Additive Manufacturing

Additive manufacturing was first developed in the late 1980s [28] and combines pieces of material, usually layer by layer, to produce a coherent part. Additive manufacturing using a variety of materials, including metal, offers more design freedom than conventional processes. It enables the production of elements with a geometry impossible to obtain with conventional technologies [29]. It was supposed to be used for prototyping, but AM has become so widespread that it is now used to manufacture finished products in industrial quantities [29]. The AM technology has gained popularity thanks to its advantages, the most important of which are: rapid prototyping, the acceleration of works in the research and development area, the production of complex elements or those impossible to produce with other technologies, the creation of ready-made elements without the need to manufacture subassemblies, no need to use many different machines, the possibility of producing elements of diametrically different shapes on one device, and the possibility of ensuring continuity of production by reprinting the missing components [30].

2.1. Additive Manufacturing Methods

According to [31], AM techniques are divided into seven elementary methods: binder jetting, directed energy deposition, material extrusion, material jetting, powder bed fusion, sheet lamination, and vat photopolymerization.

Binder jetting (BJ) was invented at the Massachusetts Institute of Technology in 1993 [32]. It consists of combining particles of dry powder with a liquid binder [33]. Layer by layer, the powder and then the binder are applied to the abruptly descending bed. This method is usually used to form elements based on ceramic powders [34], metals, biomaterials, glass, polymers, and combinations thereof [35]. Typically, phosphoric acid, citric acid, a polymer solution, or water is used as the binding material [36]. Manufactured

elements always require further treatment, such as powder removal and sintering, and are characterized by high porosity [32].

Powder bed fusion (PBF) is an additive manufacturing method that selectively heats the material powder with a laser beam or electrons [37]. The powder is fed in a controlled thickness layer by layer and fills the successive print planes. The powder is cured only at the point where the workpiece is formed, and the remainder of the powder can support inclined or horizontal surfaces that would normally require the construction of temporary support structures. Removal of the supporting structures from the confined space (e.g., limited by the walls of the exchanger) is practically impossible. The advantage of the method is that the removal of the remaining loose powder filling the voids is not a problem. Depending on the heat source (light beam, electron beam), two subgroups of solutions are distinguished: laser PBF (L-PBF) and electron beam PBF (EB-PBF) [38]. Selective laser sintering (SLS), selective laser melting (SLM), electron beam melting (EBM), and direct metal laser sintering (DMLS) are the elementary AM techniques included in the PBF method. In the former PBF technology, the working material is usually a polymer, and in the latter, a metal [39].

Directed energy deposition (DED) is an AM method in which powder or wire is fed, by means of a multi-axis system of nozzles, to the point of focusing a laser beam or an electron beam. The material, most often a metal or alloy (e.g., Ti, Co-Cr, Inconel, NiTi), in an inert gas atmosphere and at a temperature above 3000 °C, melts, and then cools down to form a compact 3D geometry [32]. The DED method eliminates the need to spread the powder over the entire layer, reducing its consumption, and the use of multiple nozzles allows for the simultaneous supply of various materials to the liquid pool. [40]. The method allows you to create large-size geometries, but requires further machining [38]. Among the methods of directed energy deposition, the following stand out: laser-engineered net shaping (LENS) [40], wire and arc additive manufacturing (WAAM) [41] and 3D laser cladding (CLAD) [32].

Material extrusion (ME), also known as extrusion free-forming (EFF), is a technique of producing 3D objects by extruding molten plastic through a moving nozzle on a step (with each printed layer), lowering the base [42]. Fused deposition modeling (FDM), also called fused filament fabrication (FFF) [43], is one of the most widely used techniques for creating objects using this method [42] and consists of extruding the molten polymer fiber through a die. Direct ink writing (DIW) and paste extrusion [39] are other techniques of this method, where the material extruded at room temperature is solidified due to thermal action or UV radiation. The shape of the detail is created by applying successive layers. Polymer resins, polymer solutions, and gels are the main materials used in this additive manufacturing technique.

Material jetting (MJ) is a method of additive manufacturing that consists of “shooting” a low-viscosity liquid, containing a solvent, a polymer, or a suspension of nanoparticles, through a nozzle onto the platform, and then drying the layers (thermal or UV rays). The main techniques for this method are drop-on-demand (DOD) and PolyJet [39]. These methods differ from each other in the number of nozzles feeding the material. Material jetting allows the application of thin layers of the working material, but cracks may form in the material as a result of drying [33].

Sheet lamination is an incremental method that creates an object by overlapping successive thin sheets of metal, paper, ceramics, and polymer. The next sheet is applied after the previous sheet of material is cut (usually with a laser). There is an adhesive layer between the sheets that allows the sheets to be joined [41], or it can be the result of applying heat (laser beam) [35]. An example of the latter method is laminated objective manufacturing (LOM) [36]. Another method of bonding is the use of ultrasound. It takes place through ultrasonic AM (UAM) technology and is used for the production of elements based on aluminum, copper, and stainless steel [32].

Vat photopolymerization is an incremental method in which a tray is inserted into a vat filled with photosensitive resin with additives (ceramic powders), to which the manufactured object will be attached. The tray moves up or down and the beam (UV radiation—

stereolithography (SLA [44–49], sometimes labeled as SL [40,43,50]); lights—digital light processing (DLP) [39]; near-infrared photons—two-photon lithography (TPL)) hardens the material.

Technology that breaks with the layer-by-layer printing convention changes its classification from vat photopolymerization to continuous liquid interface production (CLIP) [39]. In this technology, the mechanical production process, layer by layer, was replaced by a photochemical process and it hardens the resin with a UV light projected on the entire surface of the “printout”. At the same time, the areas of the resin that should not undergo polymerization are protected with oxygen fed by the printer. The image projected from the transparent bottom of the vessel with resin smoothly changes with the progress in the production of the detail. The detail is attached at the bottom to the upward-moving support and emerges from the resin bath [36]. The advantage of the CLIP method, in addition to the smooth walls of the body devoid of the features of layered additive manufacturing, is the reduction of the manufacturing time. Thanks to the projection of the image reflecting the entire contour of the object in a given cross-section, the production time of the elements can be reduced from a few hours (by the method of layered increments) to a few minutes (CLIP).

2.2. Additive Manufacturing—From CAD to CAM

The production of an element by additive manufacturing is preceded by several steps. The first is to prepare a digital three-dimensional model of an element. Using computer-aided design (CAD) software, the 3D geometry is made. There are many commercial and free CAD programs available for 3D modeling. Reverse engineering can also be used to model 3D objects. Reverse engineering is a nondestructive technology that scans existing objects with rays (typically X-rays) in order to obtain a digital image of them [28]. Most often, it requires additional actions to remove the errors that arose during scanning.

The next step is to save the model as a file whose structure is recognizable by printing devices. Usually these are files with the .STL, .OBJ, or .AMF extension.

The widely used file format is the .STL (Stereo Lithography) format. The .STL file format was developed in 1987 by 3D Systems. In the .STL file, the outer surface of a solid is represented by a mesh of planar surfaces (triangles). The more accurate the representation of a curved surface is, the greater the number of triangular surfaces, and more advanced algorithms are required to optimize the topography and reduce data processing time [51]. The disadvantages of the .STL format include: redundant data; the inability to collect data describing various materials, colors, and textures; no possibility to validate the transformed solid; the appearance of errors with the incorrect definitions of triangles; the resulting file is time-consuming to improve; and no information about units (e.g., inch/mm). Errors can arise in the process of converting the geometry to its mesh representation, as it is required to find and fill in missing triangles, make connections of missing edges, or “flip” the triangle to indicate the side on which the inner/outer space of the model is located. Repair of a model saved in .STL format is possible thanks to programs such as MeshLab, 3DPrintCloud, Netfabb, etc. The advantages of the .STL standards are simplicity (requires only standard surface triangulation algorithms); the ability to present, store, and exchange data between different devices; easy file division into smaller ones; the form has been unchanged for years (no need for additional training); implementation in almost all commercial CAD programs; and use of the format by virtually all manufacturers of AM machines. For this reason, .STL files are the most commonly used file type and are some kind of standard in AM, although this format has not yet been officially standardized [52].

The .OBJ format was developed by Wavefront Technologies. Due to the open-source license, it has been adopted by producers of CAD programs. The advantage of the format is the ability to save (in an additional file—template library .MTL) information about colors and various materials used during part printing. Thanks to the possibility of dividing the surface of the solid into polygons and the use of curves, it was possible to reduce the number of mesh elements reflecting the printed surface, which makes the file size smaller than in the case of .STL. Due to the abovementioned advantages, the .OBJ file has become

the next most frequently used 3D model data representation format in the AM industry. The biggest disadvantage of the .OBJ format is that it is more complicated, which makes it difficult to repair; this is compounded by having only a small group of programs for editing .OBJ files [53].

There is also the .AMF format, introduced in 2009. Since 2013, it has been standardized (ISO/ASTM 52915) and formally became the STL 2.0 standard. It allows you to define the surface of a solid by using curved triangles, which significantly reduced the number of planar triangular surfaces that would be required in the .STL format. In addition, it allows you to record information about the surface microstructure or a smooth transition between different types of materials. This .AMF format is far superior to the .STL format and seems to be a future-proof solution in terms of quality and quantity of stored data, but has not yet been widely implemented by AM device manufacturers. This is due to the fact that the .AMF format is undergoing constant development, and the competition for it, at the moment, is the aforementioned .OBJ format [53].

For the final preparation of the printing, the computer file containing information about the object requires further processing. In the printer's software or CAD/CAM (computer-aided manufacturing) programs, the final preparation of the printing takes place, which consists of "cutting" the geometry into layers with a thickness resulting from the technical capabilities of the printer. Additionally, printing parameters are selected, such as: printing speed, filling the space between the surfaces of the triangle mesh, designing additional supporting structures (if required), etc. This information is saved in the file in the form of a command line, the so-called G-code, which is recognizable by the printing device [39].

Performing all the abovementioned activities results in the proper preparation of the project for the production of a detail with the AM technology.

2.3. Additive Manufacturing of Lattice Structures

The use of additive manufacturing technology means that many structures/solids, previously impossible to be made with classical technologies, can be made entirely using one machine [54]. Such solids are, for example, lattice structures. Lattice structures are a system of vertices connected with each other by bars or surfaces in repeatable sections, which, in effect, form one integrated whole with a complex internal geometry. It is the complex internal geometry that makes lattice structures very often impossible to produce with traditional technologies. Lattice structures can be self-supporting or fill between the walls of the solid. The lattice filling of the solid causes a significant decrease in its mass [55,56] while maintaining stiffness [57], strength [58–60], and high energy absorption and dissipation capacity [61]. The lattice structure can be designed to exhibit different mechanical properties in different directions, making them significantly different from the properties of the material used for their production. [62]. For the abovementioned reasons, the area of application of lattice structures is becoming wider and includes: mechanical engineering [63–67], where solutions are sought to ensure lightweight structures with unchanged mechanical properties (aviation [68], architectural materials [69]), and biological engineering (bone structures [70]) and energy (construction of heat exchangers [71] with a developed heat exchange surface [72], including for waste heat recovery [73], refrigeration applications [74], thermal desalination processes [75], pool and flow boiling [76], wavy microchannel heat exchangers [77], and thermal management of electric motors [78]). Lattice structures have become an alternative to random structures (foam structures, stochastic networks). The advantage of random structures is their lightness and strength, but the disadvantage is the lack of repeatability. Additive manufacturing enables the production of structural elements designed on the basis of randomness algorithms. A review of methods for creating controlled stochastic networks is presented in paper [72].

The process of designing lattice structures consists of using the results of experimental research and computer simulations, which show the influence of the type of material, manufacturing techniques, geometry, or the volume fraction of a structure on its physical,

mechanical, and acoustic properties [79,80]. The engineer optimizes the topology according to his own requirements: minimal weight, high surface area to volume ratio, maximum rigidity, high permeability, high thermal conductivity, large solid–liquid contact area, etc. [81].

An interesting example of surface lattice structures are the so-called triple periodic minimal surfaces (TPMSs). These structures have a stiffness greater than that of other lattice structures of comparable mass [82–84].

3. Triple Periodic Minimal Surface (TPMS)

3.1. Minimal Surface

Observation of the behavior of soap bubbles shows that a film stretched between two identical, parallel circles will not form the shape of a cylindrical surface. The resulting soap film is characterized by a gradually decreasing circumference, the smallest of which is halfway between the circles. The resulting surface is a catenoid with the smallest possible surface resulting from the union of circles. The mathematical description of the catenoids was presented in the 18th century by Euler [85]. A characteristic feature of the catenoids is that at any point on its surface, you can locate two planes perpendicular to each other, which will form characteristic curves at the intersection with the surface of the catenoids. One corresponds to the curvature (k1) along a circle passing through this point and the opposite corresponds to the curvature (k2) lying on the catenoid forming. From a mathematical point of view, a catenoid is a surface whose main, mutually perpendicular curvatures at any point take the mean value 0.5 (k1 + k2) equal to zero [42]. Other minimal surfaces satisfying this dependency are, for example, helicoid, gyroid, Fisher–Koch, Neovius, and Costa surfaces.

Table 1 presents the mathematical equations of the sample minimal surfaces and their visualization.

Table 1. Examples of minimal surfaces (name, surface view, and mathematical notation).

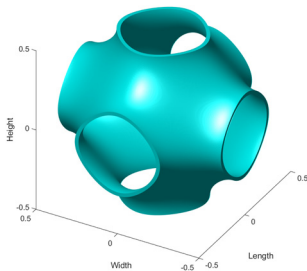
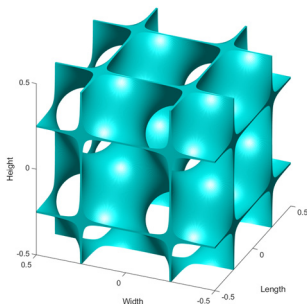
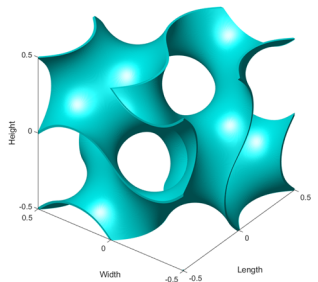
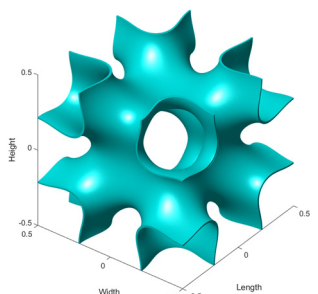
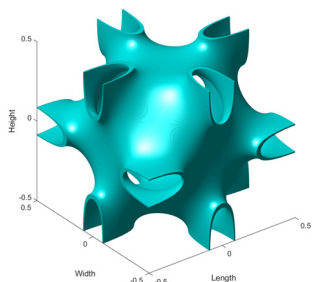
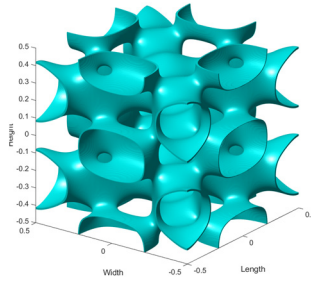
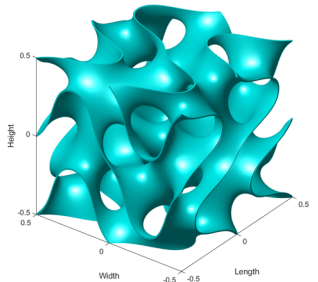
Minimal Surface	Formula	View
Schwartz primitive [86]	$f(x,y,z) = \cos(x) + \cos(y) + \cos(z) = C \quad (1)$	
Schwartz diamond [87]	$f(x,y,z) = \cos(x) \cdot \cos(y) \cdot \cos(z) - \sin(x) \cdot \sin(y) \cdot \sin(z) = C \quad (2)$	

Table 1. Cont.

Minimal Surface	Formula	View
Schoen gyroid [88]	$f(x,y,z) = \cos(x) \cdot \sin(y) + \cos(y) \cdot \sin(z) + \cos(z) \cdot \sin(x) = C \quad (3)$	
Schoen I-WP ("I-graph"- "Wrapped Package-graph") [50]	$f(x,y,z) = 2(\cos(x) \cdot \cos(y) + \cos(y) \cdot \cos(z) + \cos(z) \cdot \cos(x)) - (\cos(2x) + \cos(2y) + \cos(2z)) = C \quad (4)$	
Neovius [32]	$f(x,y,z) = 3 \cdot (\cos(x) + \cos(y) + \cos(z)) + 4 \cdot (\cos(x) \cdot \cos(y) \cdot \cos(z)) = C \quad (5)$	
Schoen F-RD [42]	$f(x,y,z) = 4(\cos(x) \cdot \cos(y) \cdot \cos(z)) - (\cos(2x) \cdot \cos(2y) + \cos(2y) \cdot \cos(2z) + \cos(2z) \cdot \cos(2x)) = C \quad (6)$	
Fischer-Koch S [42]	$f(x,y,z) = \cos(2x) \cdot \sin(y) \cdot \cos(z) + \cos(x) \cdot \cos(2y) \cdot \sin(z) + \sin(x) \cdot \cos(y) \cdot \cos(2z) = C \quad (7)$	

In Equations (1)–(7), the quantities x , y , z are the spatial coordinates and C is the constant. When the constant C takes the value $C = 0$, it means that the minimal surface thickness is 0, and thus, its volume is equal to 0 (Figure 1a), and the entire space is divided into two equal parts. When the constant C assumes the value of $C \neq 0$, then the isosurfaces

are separated [89] by a distance of $2C$ ($+C$ and $-C$) (Figure 1b). Filling the space between isosurfaces with AM techniques is the basis for producing solids based on minimal surfaces.

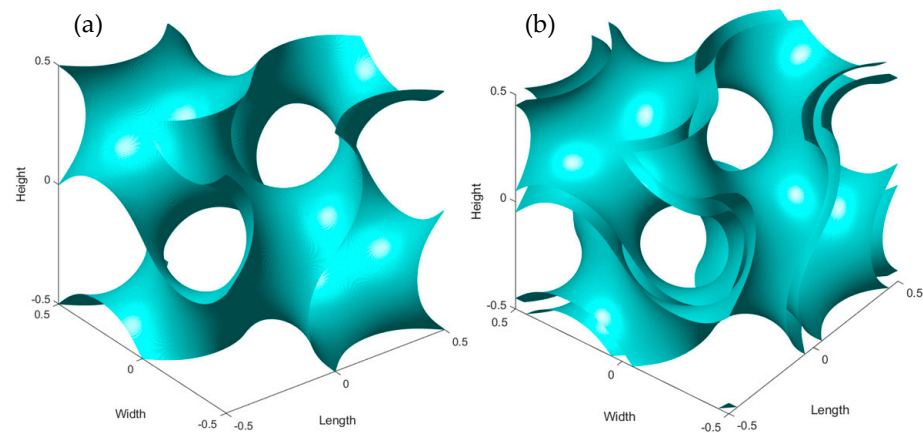


Figure 1. Minimal surface—gyroid: (a) isosurface with constant $C = 0$ (according to Formula (3) from Table 1); (b) isosurfaces spaced apart by the amount of $\pm C$.

3.2. From Minimal Surface to TPMS

The first description of the minimal surface, dating back to the 19th century, was given by Schwartz and Neovius. The minimal surface of an infinite size, created by duplicating the elementary formation in three main directions, is called the triply periodic minimal surface (TPMS) [42]. TPMSs are mathematically defined smooth (without edges or angles) surfaces that are infinite in 3D space [90], and which are divided into two intertwined infinite volumes [91]. The TPMS was created on the basis of Schwartz's concept (1885), the TPMS Schwartz diamond (Figure 2).

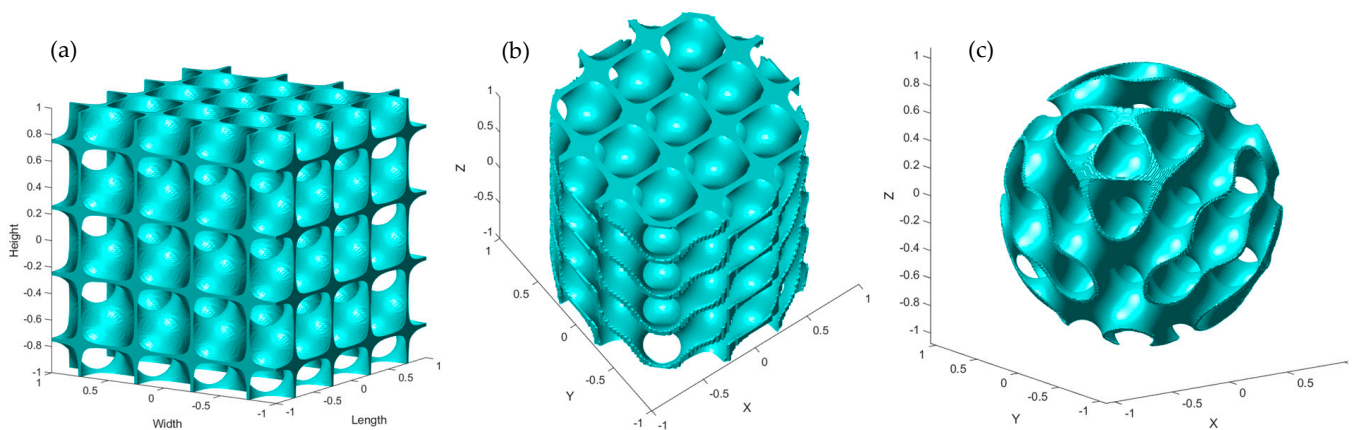


Figure 2. TPMS created on the basis of the Schwartz diamond minimal surface in a limited space: (a) cuboid, (b) cylinder, (c) sphere.

Figure 2 shows examples of TPMSs (Schwartz diamond or “diamond” for short) contained in the space of a cuboid, cylinder, and sphere.

In additive manufacturing, the TPMS is a surface that has a certain thickness. This means that the constant C , in Formulas (1)–(7), is a value different from 0. The interface (wall) separates two domains, e.g., two fluids. The greater the wall thickness, the greater the relative density of the TPMS. The effect of wall thickness on the relative density of the TPMS (gyroid) is shown in Figure 3.

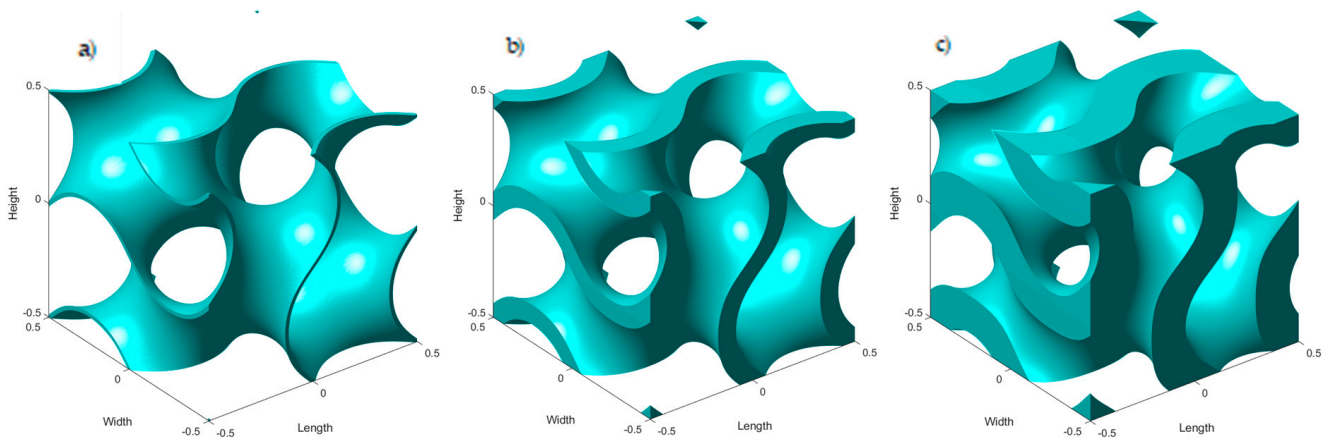


Figure 3. TPMS, gyroid, of relative density: (a) 5%, (b) 25%, (c) 45%.

The TPMS structure shown in Figure 3 is the so-called sheet network [92], where the wall separates two domains. Another variation of the TPMS structure is the so-called solid network [83]. A solid network TPMS is created when one of the domains is replaced with a solid. Then, there is a structure composed of a solid body and a space that one fluid can flow through. An example of the structures of TPMS sheet and solid types is shown in Figure 4.

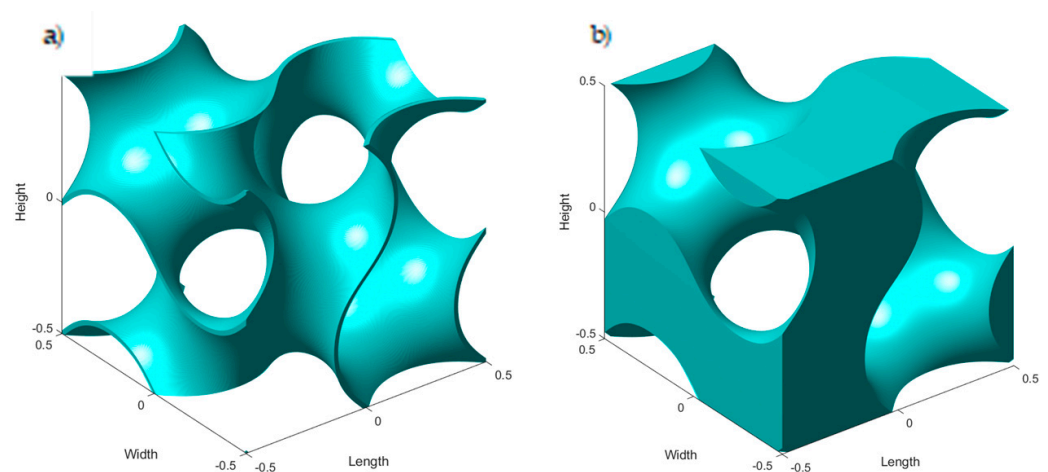


Figure 4. Gyroid structure types: (a) sheet network, (b) solid network.

Formulas (1)–(7) contained in Table 1 express the mathematical notation of the minimal area, which, with minor modifications, can be used to describe the TPMS. For example, Formula (3) on the surface of the character's gyroid:

$$f(x,y,z) = \cos(x) \cdot \sin(y) + \cos(y) \cdot \sin(z) + \cos(z) \cdot \sin(x) = C,$$

can be transformed to form:

$$f(x,y,z) = \cos(2\pi x/L_x) \cdot \sin(2\pi y/L_y) + \cos(2\pi y/L_y) \cdot \sin(2\pi z/L_z) + \cos(2\pi z/L_z) \cdot \sin(2\pi x/L_x) = C. \quad (8)$$

The obtained Formula (8) describes the TPMS based on a gyroid, where the sizes, L_x , L_y , L_z , denote the size of the minimal surface elementary cell. By changing the value of the constant C (the thickness of the TPMS wall, and thus, its relative density) and the size of the elementary cell of the minimal surface area, TPMS structures with a heterogeneous structure are obtained [93]. The effect of relative density and the size of the primary minimal surface cell on the TPMS geometry is shown in Figure 5. The first structure (Figure 5a) is a homogeneous TPMS structure based on a gyroid and the number of elementary cells

$2 \times 3 \times 5$, where 2, 3, and 5 are the numbers of repetitions of the minimal surface along the principal directions. The structure shown in Figure 5b shows a modified variant of the initial structure, in which the wall thickness (relative density TPMS) is subject to a smooth change (from 10% to 50%). Figure 5c illustrates the effect of changing the size of the elementary minimal area cell on the TPMS geometry. In the analyzed case, the size of the elementary minimal surface cell was doubled.

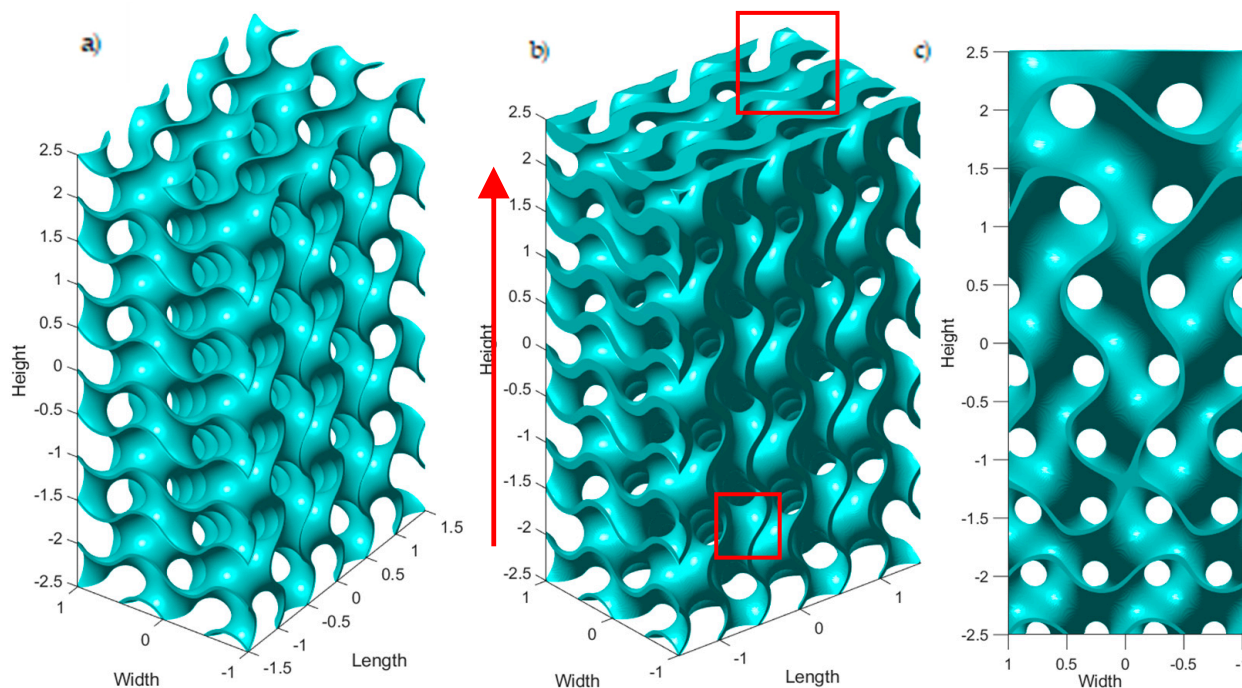


Figure 5. The structure of TPMS (gyroid) with dimensions $2 \times 3 \times 5$: (a) homogeneous structure, (b) relative density increases from 10% to 50%, (c) the size of the elementary cell of the minimal area increases twice (relative density—10%).

Independent preparation of TPMS geometry in CAD programs is difficult, and due to the development of AD techniques, solutions based on minimal surfaces are becoming more and more popular. As a result, many free programs have been created to facilitate the automation of TPMS geometry creation. Programs in this category include: MSLattice [94], Minisurf [95], TPMS Designer [96], and FLatt Pack [81]. These programs allow you to prepare various TPMSs and export them to the STL format, recognizable in all CAD programs. Due to the growing demand for TPMS manufacturing with AD methods, there have also been extensions that facilitate the automation of TPMS geometry preparation in commercial CAD programs. These programs include: Autodesk Fusion 360, nTopology [97,98], and CREO Parametric [55,99].

To sum up, it can be stated that the triply periodic minimal surface: (a) can be described by an algebraic equation, and therefore, is an isosurface; (b) is a structure that repeats periodically in three independent directions; (c) is a minimal surface, with no edges and no angles; (d) is characterized by great freedom in modifying the wall thickness (relative density) and the size of the elementary cell; and (e) the production of the TPMS with additive methods requires the discretization of the geometry by reflecting its external surfaces with a grid of triangular flat surfaces [50].

4. Heat Exchange with TPMS

There are reports in the literature of metal-printed heat transfer devices with lattice structure elements in their structure. Typically, these structures are not complicated and

do not require TPMS modeling skills or the ability to use programs that automate the design processes.

The results of experimental studies of a 10×10 mm crosscurrent heat exchanger with a lattice-rod structure are described in paper [100]. It was found that the exchanger is characterized by an increased value of the heat exchange in relation to the volume unit of the exchanger.

A printed, copper mini-heat exchanger consisting of collectors and a section of parallel tubes with an internal diameter of 1.60 mm placed between them is described in paper [49]. Hot water flowed through the channels, and the exchanger itself was placed in the wind tunnel. The potential of 3D printing techniques to produce mini-heat exchangers with various channel configurations has been found.

Further exemplary works describing the advantages of developing the contact surface of the working fluid with the wall (not the TPMS) produced by AD techniques are published in these papers: [101] (lattice structure); [102] (porous open-cell aluminum foam), [103] (compact heat pipe); [104,105] (transferring heat from Kelvin's tetrakaidecahedron foam to the air); [106] (octet, D-cube, tetrakaidecahedron, and cube); [107] (tube with longitudinal ribs); [108] (pin fin arrays in annular channels); [109] (membrane); [110,111] (inserts turbulating the flow of the medium in the pipe); and [112] (study of the thermal conductivity of AlSi10Mg formed as a result of powder fusion of the bed and modified with heat treatment).

These studies indicate that the process of heat exchange between the fluid and the printed wall requires research, as the heat transfer coefficients differ from the values obtained during heat transfer from walls produced with classical methods.

4.1. Heat Dissipation and Heat Sink

Paper [93] describes the results of a CFD simulation of heat transfer and air flow resistance in contact with the TPMS. The finite volume method using direct pore-scale simulations (ANSYS Fluent 2019 R2) was used to solve the problem. The solid network channels were created on the basis of the minimal surfaces of the primitive, gyroid, diamond, and Schoen I-WP types. The flow took place along the TPMS with the architecture of $1 \times 1 \times 8$ ($2.54 \text{ mm} \times 2.54 \text{ mm} \times 20.32 \text{ mm}$). The tests were carried out in the range of $Re = 10\text{--}129$ and porosity $\varepsilon = 20\% \div 80\%$. A laminar model was employed to solve the governing equations for the study conditions. It was found that the flow resistance increased with increasing Re and was the lowest for the flow along the primitive structure, followed by the gyroid and I-WP, and was the highest ($Re = 100$, which was as much as 36 times higher) for the flow along the diamond structure. The mean Nusselt number increased as the Re number increased. Similarly to the flow resistance, the value of the Nu number reached was successively higher for the structures: primitive, gyroid, I-WP, and diamond. Relating the increase in the heat transfer coefficient to the flow resistance, it was found that the optimal design is channels based on I-WP, for which the thermal efficiency related to the unit flow resistance was 1.9 times higher than for the diamond-type channel. The Nu number was positively influenced by the increase in the TPMS porosity value.

In [29], the results of a CFD simulation of flow resistance and heat exchange through a channel with an internal diameter of $d = 10$ mm were compared with the results of a simulation of flow through TPMS channels (sheet network) with the structure of $1 \times 1 \times 5$ ($10 \text{ mm} \times 10 \text{ mm} \times 50 \text{ mm}$). Ducts with a gyroid and primitive filling were designed. The relative density range was 0.15 to 0.4. Water flowed through the channel ($Re = 7.4 \div 98.3$), which received heat from isothermal surfaces. OpenFOAM v1812 software with a conjugate heat transfer solver was used to model fluid and heat transfer. The Reynolds-averaged Navier–Stokes (RANS) method and the $k\text{--}\varepsilon$ model were used to model turbulence. It was found that the flow through the TPMS channels gives values of the heat transfer coefficient that are an order of magnitude higher than those from the flow through the circular channel. However, they are accompanied by a significant increase in fluid flow resistance. Similar to the work from [93], the gyroid-based TPMS channel flow gave a higher Nu value than along the primitive structure, but also had a higher value of the unit flow resistance.

The flow through a cuboid with a TPMS (gyroid) filling and a lattice-rod structure was subjected to CFD tests in order to determine the resistance to fluid movement [113]. Ansys Fluent was used to predict the pressure drop. Water flowed in the amounts of 2, 4, 6, and 8 mL/min with the $3 \times 3 \times 3$ structure and with a porosity of 65% ÷ 90%. The base TPMS cell size was varied, ranging from 880 μm to 2890 μm . It has been found that for the same water flow rate and the same porosity, the flow resistance of the TPMS is 50% higher compared to the flow resistance of the lattice structure.

A countercurrent heat exchanger based on a sheet network TPMS (Schwarz primitive, Schwarz diamond, and Schoen gyroid) and a geometry equal to one elementary TPMS cell (12 mm \times 12 mm \times 12 mm) was investigated numerically in work [90]. The software Star-CCM+ [54] with the SIMPLE (Semi-Implicit Method Pressure Linked Equations) algorithm was used to numerically solve the Navier–Stokes equations. Laminar flow of working fluids was assumed. The heat transfer coefficients and the flow parameters of the exchanger were assessed. It was found that the diamond structure allows for the highest Nu number values, but also, the flow resistance per unit length of the exchanger is the highest in this case. As in the previously cited studies, based on the increase in Nu compared to the increase in flow resistance, the diamond-type structure is the recommended structure for the construction of heat exchangers using AM methods.

In paper [114], the influence of the TPMS on heat transfer and water flow resistance in the structure of the sheet gyroid that was $2 \times 2 \times 10$ (10 \times 10 \times 50 mm) was numerically investigated. StarCCM+ 2019.2 software and the volume-averaged model were adopted to solve the momentum and energy transfer. Six different values of water velocity in the range of 0.001 ÷ 0.006 m/s ($\text{Re} = 3.6 \div 21.6$) and the initial temperature of 20 $^{\circ}\text{C}$ were assumed as the boundary conditions for the simulation of the flow along the isothermal surface of the gyroid ($T_s = 25 \text{ }^{\circ}\text{C}$, $T_s = 50 \text{ }^{\circ}\text{C}$, $T_s = 75 \text{ }^{\circ}\text{C}$). It was found that the heat transfer coefficients have values similar to the values obtained for other periodic structures described in the literature.

The numerical study of fluid flow through a gyroid (1 \times 1 \times 1) sheet network structure using the lattice Boltzmann method is described in paper [115]. The structure with a porosity of 0.1–0.9 was used to flow fluids whose Reynolds number changed from $\text{Re} = 1.2$ to $\text{Re} = 5046$. The authors noticed that the mass transport on one side of the surface did not reach the same parameters as on the other side of the separating domain. The authors show the need to adjust the printing parameters in such a way as to ensure the possibility of printing the exchanger walls without micropores.

In further CFD research [116], they set the conditions of the heat exchange and air flow resistance to be an initial temperature of 0 $^{\circ}\text{C}$ through a 10 \times 10 \times 70 mm channel with a TPMS sheet network (diamond) with the dimensions 10 \times 10 \times 10 mm (porosity 59%, 66%, 76%, and 88%), which was placed inside. One of the TPMS walls was in contact with an isothermal surface on the channel wall. This surface had a temperature of 40 $^{\circ}\text{C}$. The OpenFOAM was utilized to solve the temperature and the flow field in the channel using a conjugate heat transfer model called multiregion simple foam. The solver discretizes the equations using the finite volume method (FVM), and by applying the SIMPLE algorithm, implicitly couples the pressure to the velocities. It was shown that the application of the TPMS increased the heat exchange between the isothermal surface and air, and it was greater the thicker the wall of the gyroid. The structure with a porosity of 59% showed a 250% greater performance when compared to a structure with a porosity of 88%. The authors also described the results of structure optimization in their next article [117].

Research using CFD (Simcenter Star-CCM software) and free convection from TPMSs (gyroid and diamond) in the form of a sheet network and solid network is described in paper [118]. The finite volume method using Simcenter STAR-CCM+ software and the Reynolds-averaged Navier–Stokes (RANS) turbulence model were used to solve the simulation. TPMS geometries with a porosity of 0.80 and dimensions of 22 \times 32 \times 22 (mm) were placed in a partially limited space (limited from the bottom by the base area). The simulated heat source (0.5 W and 2.1 W) acted on the TPMS surface in contact with the base.

The simulation results showed that the TPMS-based heat exchanger operating under free convection conditions is able to dissipate 48–61% more energy than a traditional pin-fin heat sink.

Seven different TPMS geometries were used to numerically estimate the flow resistance and heat transfer coefficient during the flow of water through a TPMS-filled channel with a $1 \times 1 \times 4$ structure [119]. Hydraulic properties of the structures were computed using the laminar flow physics solver in COMSOL. It has been shown that compared to the laminar flow of water through pipes, the application of a TPMS causes an increase (by an order of magnitude) in the coefficient of friction, but also an increase in the Nu number. The increase in Nu was greater the higher the Re of the flowing fluid was. Comparing the TPMS structures with each other, it was found that TPMS primitive increased the Nu value the least. The diamond-type structure turned out to be the best. The authors showed that a TPMS diamond heat exchanger would be 3–10 times smaller than a conventional tubular exchanger.

A heat sink based on a TPMS (gyroid, Figure 6) and diamond TPMS, with a number of repetitions of the elementary cell and with a minimal surface area of $2 \times 2 \times 3$, was investigated experimentally and numerically by the authors of paper [83]. A sheet-network and solid-network heat sink with dimensions of $20 \times 20 \times 30$ mm and a porosity of 80% were placed in a channel with a cross-section of 20×20 mm. Air flowed through the channel at an ambient temperature, at an average speed of $1.5 \text{ m/s} \div 5.5 \text{ m/s}$. The temperature of the bottom surface of the heat sinks was constant at $80 \text{ }^\circ\text{C}$. The STAR-CCM+ platform using the Reynolds-averaged Navier–Stokes (RANS) method coupled with energy for the flow velocity and temperature field solutions was used. The realizable $k\text{-}\epsilon$ model was used for turbulence modeling. The results indicated that, due to the highest surface area density, the gyroid-sheet structure had the lowest thermal resistance and the highest heat transfer coefficient.



Figure 6. View of the gyroid structure made using the AM method for the study of heat transfer under forced convection conditions [83].

An element with the shape shown in Figure 7 was used as an insertion into the pipeline to improve the mixing of the flowing medium [120]. Using the CFD simulation, the influence of the insert (gyroid TPMS with 10 different porosities) on the fluid flow resistance and heat transfer from the insert to the flowing fluid was investigated. ANSYS Fluent was used for carrying out simulations. The ten different dimensions of the gyroid variants had large contact surfaces with the fluid despite their small dimensions. In the best design variant, the number of Nu was increased by 343% compared to the empty pipe.

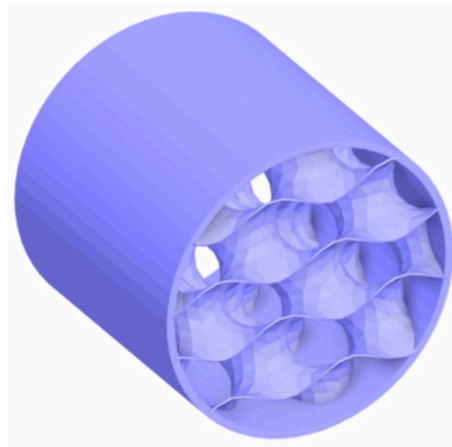


Figure 7. View of the gyroid structure made using the AM method for the study of heat transfer under forced convection conditions [120].

Three TPMSs (gyroid, primitive, I-WP) and a Kelvin cell (as reference) were used to fill the space occupied by the phase change material (PCM) [121]. The purpose of this filling was to distribute heat in the volume of the PCM. PCM is characterized by a low thermal conductivity coefficient, which is a disadvantage of this material as a heat store. The TPMS and Kelvin cells with a structure of $1 \times 1 \times 4$, dimensions of $7 \times 7 \times 28$ mm, and a porosity of 90% conducted heat under conditions of constant heat flux or an isothermal surface, causing the melting of the PCM. ANSYS FLUENT 18.0 was used to solve the governing equations. Through transient CFD simulations, it was shown that the time needed for the complete phase transformation of the PCM was 31% shorter for the gyroid structure, 35.3% shorter for the primitive structure, and 40.3% shorter for the I-WP with respect to the filling of the Kelvin cell structure. It is worth emphasizing that these times were incomparably shorter than the times that would be required if the PCM did not have a metal filling. The extended research and the conclusions drawn were confirmed in other articles by the authors of [56,122,123]. The positive aspects of using a TPMS to improve heat transport in a PCM are also described in paper [124].

4.2. Heat Exchangers

Paper [125] presents the concept of a water heater connected to a washing machine. An electric heater is placed in a specially shaped elbow (Figure 8) with an internal structure of a TPMS (gyroid), which is a developed heat exchange surface and a water flow turbulizer. The authors emphasize the high efficiency of the implemented construction solution.

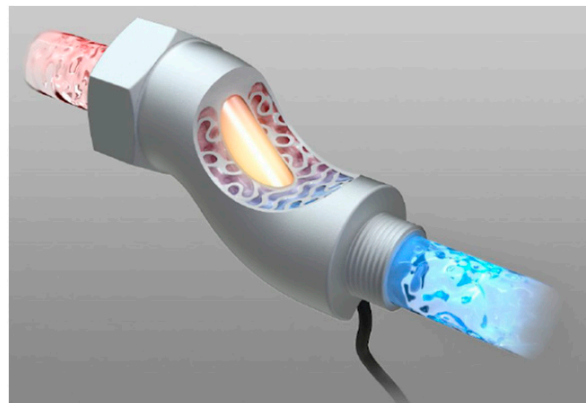


Figure 8. View of the heat exchanger for heating the water supplied to the washing machine [125].

Paper [87] presents the results of the experimental research on the crossflow of an air-to-air heat exchanger. The exchanger is based on the shape of a cuboid with dimensions

of $114 \text{ mm} \times 114 \text{ mm} \times 114 \text{ mm}$. The exchanger space was filled with a gyroid, primitive, and diamond sheet network with a relative density in the range of $0.77 \div 0.90$. The air temperature at the inlet of the exchanger was $40 \text{ }^\circ\text{C}$ (warm air) and $20 \text{ }^\circ\text{C}$ (cold air). The air flow rate was changed in the range of $0.005 \div 0.015 \text{ m}^3/\text{s}$. It was found that the heat exchanger based on the TPMS diamond type had the highest efficiency (about 50% with a relative density of 0.79). Unfortunately, it was also characterized by the highest flow resistance. It was noticed that the heat exchangers used on the test stand with a wall thickness of 0.16 mm, made with the fused deposition modeling (FDM) method, had leaks between the partitions. An alternative method of making the exchangers was proposed (selective laser sintering—SLS method).

The results of the research on a heat exchanger for cooling the oil used to lubricate turbine engine bearings made with AM technology are presented in paper [126]. It was assumed that the prototype structure would have the same thermal and flow parameters as the original heat exchanger. The assumption was fulfilled, and the prototype was 66% lighter and 50% smaller than the original design.

The work in [127] describes the results of a CFD simulation of heat exchange and flow resistance in prototype heat exchangers, in which the channels inside the casing had a geometry based on a TPMS of the gyroid (Figure 9a), primitive (Figure 9b), and diamond (Figure 9c) type. From the analysis of the obtained results, the authors concluded that the highest values of the Nu number were obtained for the exchanger with gyroid-shaped channels. Using the primitive structure resulted in lower Nu values, but this structure also had the lowest flow resistance values. Relating the intensity of heat exchange to the unit flow resistance, the exchanger with the primitive structure turned out to be the optimal design.

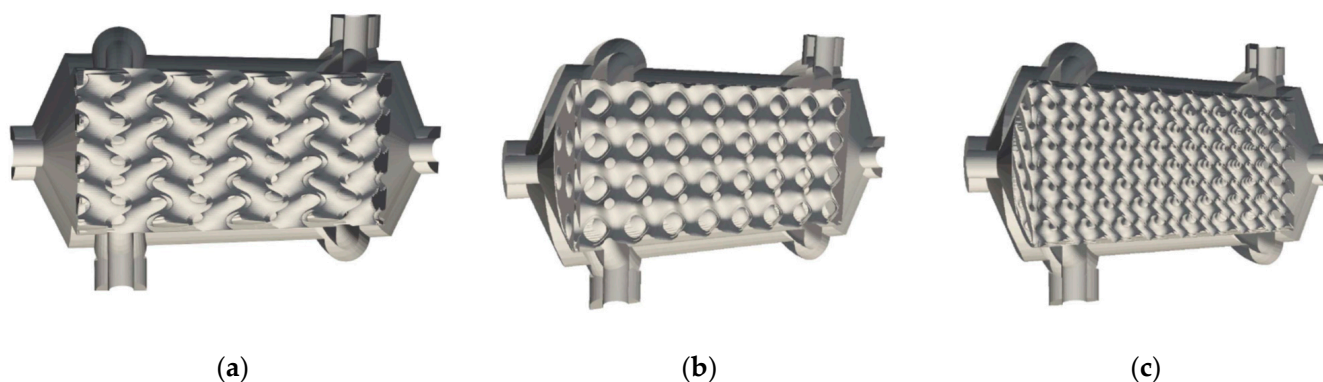


Figure 9. A cross-section through a heat exchanger in the research of [127].

A new method of designing TPMS-based heat exchangers with virtually any channel structure was presented in [47]. Designing enables the use of the obtained models for both CFD simulation and 3D printing. Examples of proposals of various possible design solutions proposed by the authors are listed in Table 2. Additionally, the authors printed monolithic aluminum heat exchangers (Figure 10) with dimensions of $150 \times 75 \times 60 \text{ mm}$ for four different filling options: a traditional plate and a TPMS that is $16 \times 8 \times 4$ with a structure of primitive, gyroid, or diamond. The flow resistance and overall heat transfer coefficient of the exchanger during the flow of hot ($40 \text{ }^\circ\text{C}$) and cold ($17.5 \text{ }^\circ\text{C}$) water in the amount of $0.06 \div 0.15 \text{ kg/s}$ were determined. It has been shown that the heat exchangers based on TPMSs are similar to each other in terms of thermal efficiency and are characterized by a higher overall heat transfer coefficient in relation to the plate exchanger. For the diamond structure, it was even 100% higher.

Table 2. View of design proposals for heat exchangers according to [47].

Heat Exchanger Type	General View
L-shaped T-shaped	
U-shaped with different positions of connection nozzles	
Spiral-shaped (structure: primitive, gyroid, diamond)	
C/O/S/W-shaped	
coil-shaped (structure: primitive, gyroid, diamond)	

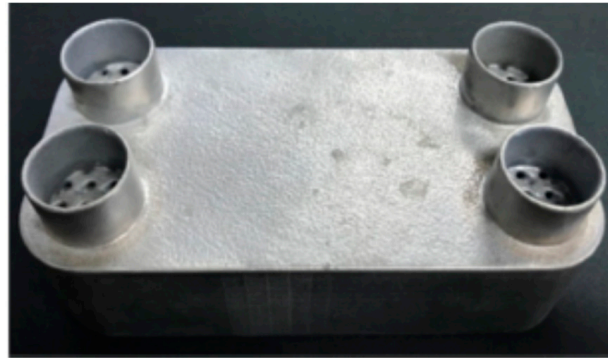


Figure 10. View of a heat exchanger printed in metal in research [47].

The 3D model of the crosscurrent heat exchanger with inlet channels adapted to the shape of the TPMS used (gyroid and diamond, $2 \times 2 \times 2$) was subjected to numerical tests to assess the values of: flow resistance, heat transfer coefficient, and temperature changes of the flowing medium [128]. Hot ($T = 82 \text{ }^\circ\text{C}$) and cold ($T = 27 \text{ }^\circ\text{C}$) water flowed through the exchanger in the amount of 0.00092–0.023 kg/s. It was found that by assuming that the heat exchanger is made of aluminum alloy AlSi10Mg, the highest heat transfer coefficient ($1413 \text{ W}/(\text{m}^2 \text{ K})$) was obtained for the diamond structure.

The countercurrent water- CO_2 heat exchanger was the subject of the simulation analyses described in paper [129]. Two constructions were compared: the TPMS (gyroid) and the proprietary printed circuit heat exchange solution. It was found that the TPMS-based heat exchanger has better flow and thermal properties in relation to the proprietary design.

The shell-and-tube heat exchanger (Figure 11) was the subject of research by the authors of [130]. The dimensions of the specific heat exchange zone were $50 \text{ mm} \times 50 \text{ mm}$. Water flow ($0.0083 \div 0.15 \text{ kg/s}$) took place through channels formed by gyroid and diamond structures. The base TPMS cell was sized to flow through eight interleaved channels. Since similar thermal parameters of the heat exchange process were obtained, it was assumed that the diamond structure (due to simpler modeling) was more suitable for the production of heat exchangers by hypertrophic methods, although the gyroid was characterized by slightly higher values of the ratio of exchanged heat to flow resistance.

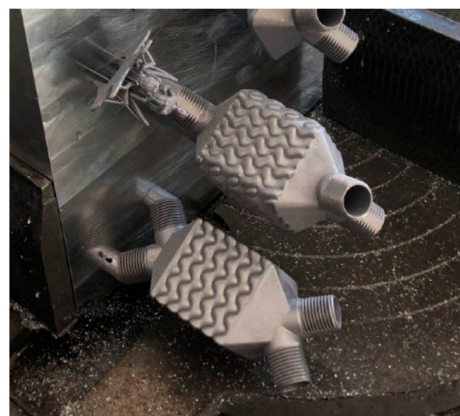


Figure 11. View of the heat exchangers used in the research by the authors of [130].

The crosscurrent heat exchanger (Figure 12), based on the TPMS gyroid type, was the subject of the experimental research and CFD simulations described in [48]. The actual heat exchange area consisted of $7 \times 7 \times 7$ elementary structure cells with a side length of 4.6 mm and with a relative density of 20% (porosity 80%). Hot and cold water flowed in the amount of 0.0016–0.0045 kg/s. Depending on Re, the value of the heat transfer coefficient was 120–160 $\text{W}/(\text{m}^2 \text{ K})$. The authors state that a 55% increase in the efficiency of

the exchanger was achieved compared to a thermodynamically equivalent exchanger, but the proposed solution was 90% smaller in size.

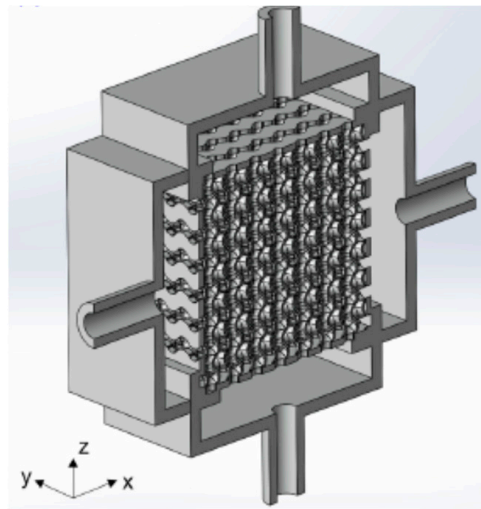


Figure 12. Cross-section through the heat exchanger used in CFD and experimental studies in work of [48].

The concept of using a TPMS (primitive) for the shaped flow of water cooling a battery pack (Figure 13) is described in [86]. Experimental studies and CFD showed that the maximum temperature of the battery pack was reduced by about 60 °C relative to water cooling in the conventional straight tube.

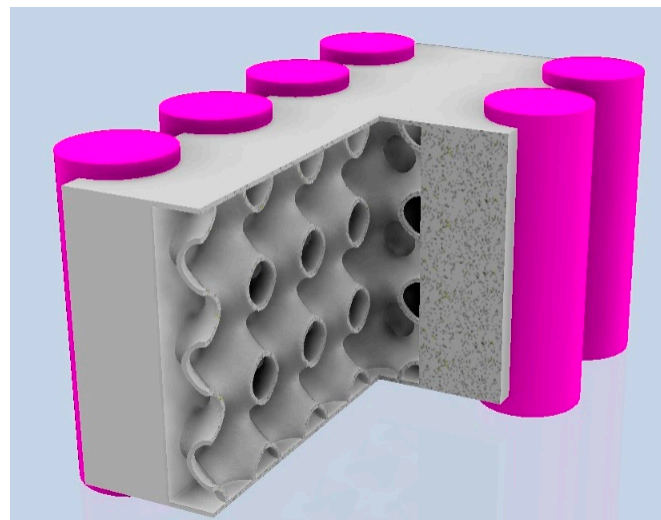


Figure 13. Cross-section of the channel shaping the flow of water cooling the battery pack—pictorial drawing.

The presented literature review shows that the minimal surfaces are gradually also being used in heat exchange. Mainly, theoretical works dominate, and the benefits of using TPMSs in heat exchange are mainly confirmed by the results of CFD simulations. The few experimental studies described in the publications exhibit the need for further experimental studies to deepen the knowledge about heat transfer coefficients and fluid flow resistance in contact with TPMSs. Optimization of the structure, undeniably characterized by higher heat transfer rates, requires taking into account the energy expenditure on the operation of devices, forcing the flow under conditions of increased flow resistance.

5. Conclusions

The literature review on the possibility of using TPMSs to create heat transfer devices shows the following important facts:

1. A huge number of publications devoted to the minimum space and its extensive version in space (triplly periodic minimal surface) concern numerical simulation tests and cover the issues of resistance to static and dynamic loads, internal stress distribution, strength limit, stability, etc.
2. The development of additive manufacturing techniques seems to be a common technique for the production of TPMSs and elements containing TPMSs, which makes it possible to publish the results of experimental research and verify the results of numerical simulations. The number of publications devoted to the results of experimental TPMS strength tests is systematically increasing.
3. The minimal surface is a type of geometry that is only just being used in the field of thermal engineering and the number of publications devoted to this subject, thus far, is very limited.
4. Most of the papers devoted to the possibilities of using TPMSs in the area of heat transfer present the results of fluid dynamic simulations (CFD), mainly with the use of minimal structures only.
5. Practically, apart from a dozen or so publications, there are no publications devoted to experimental studies of real heat exchange devices with a TPMS as a heat exchange surface.

From the few available CFD data sources and the sporadic results of experimental studies on heat transfer and fluid flow in TPMS-based heat exchangers, it is concluded that:

1. Out of dozens of possible TPMSs, thus far, only four have been subjected to CFD and experimental tests: primitive, gyroid, diamond, and I-WP.
2. The use of TPMSs in heat transfer, on the one hand, increases the average Nu value several times compared to channels with a circular cross-section or a flat surface, but on the other hand, it increases the flow resistance.
3. Flow resistances in channels created on the basis of TPMSs depend, among other things, on the TPMS geometry and having the same geometric parameters (overall dimensions, number of elementary minimal surface cells, relative density) and flow resistances; the lowest flow resistances were obtained for the primitive TPMS, then gyroid, I-WP, and diamond TPMSs.
4. The highest increases in Nu were recorded for diamond, I-WP, and gyroid surfaces, followed by the primitive structure.
5. According to many authors, the TPMS based on the diamond structure seems to be the most promising when taking into account the ease of design of the exchanger and the improvement of thermal efficiency in relation to the flow resistance.
6. Further research (especially experimental) on the use of TPMSs in heat exchangers is needed, as the current state of knowledge is not supported by a sufficient number of publications.

The literature review shows that there is a huge range of potential further actions in the area of TPMSs and their possible applications in heat transfer. These possibilities should be considered in several areas:

- CAD: It is required that the developers of commercial CAD programs foresee the possibility of automating the creation of TPMSs in order to easily create heat exchangers while minimizing the file size. It is required to enter as many known TPMSs as possible or to be able to define the TPMS functions yourself. The authors' own experience shows that the use of geometry exported to the .STL format from free software severely limits the creation of exchangers with nonstandard shapes.
- CAM: Trials of printing in metal, especially copper and aluminum, should be carried out in order to gain knowledge about the advantages and disadvantages of each of the AM methods. Then, it will be possible to indicate a proven, dominant, and

recommended method for heat transfer. It is expected that we will be able to print exchangers with user-defined roughness, smoothly reflecting the curvature of the minimum surface. It should provide a printout of the exchanger that will be pressure-resistant, will not adversely affect the substances used as a working fluid (e.g., paraffin, refrigerants), and have a continuous structure that prevents uncontrolled mass transfer through the partition, etc.

- CFD: In this regard, it is expected that we will be able to conduct simulation tests of both heat transfer coefficients and flow resistance using the most numerous representation of TPMS shapes. As a result, it will be possible to identify a TPMS that will direct future experimental research on the TPMS shapes recommended on the basis of comparative analyses. They should be characterized by both a high heat transfer coefficient and low flow resistance. It should be stated which TPMS and what size of the basic cell or porosity should be characterized by the developed heat exchange surfaces, both during flow and during free convection/forced convection/phase changes (boiling, condensation, melting, and crystallization).
- Experiment: Currently, experiments are the least described activity in the area of heat transfer with the use of TPMSs. It would be advisable to conduct basic research, in addition to the research of structures, dedicated to the purpose of specific applications. The aim should be to obtain knowledge about the flow resistance and heat transfer coefficients between the fluid and the printed surface (flat, cylindrical), as well as the developed TPMS surface. Consequently, it is expected that experimental tests will be conducted using the ribbed external/internal side of the partition (TPMS). In the next step, the basic structures of heat exchangers known for heat transfer should be modified and tested. It would be necessary to demonstrate the potential possibilities and limitations of the use of exchangers in the broadly understood low- and high-temperature power industry, providing the basis and setting directions for their conscious design.

Bearing the above in mind, one should be aware that the further development of AM with the use of TPMSs in heat transfer requires an interdisciplinary approach to the field and requires the cooperation of material science specialists, CAD designers, additive manufacturing technologists, and the scientific community to explore, theoretically and experimentally, the use of CDF knowledge in the field of mechanic fluids and heat transfer.

Funding: The research was funded by the Polish National Science Center, grant number: 2021/05/X/ST8/00023.

Data Availability Statement: Not applicable.

Conflicts of Interest: The authors declare that there are no conflict of interest.

References

1. Sefene, E.M. State-of-the-art of selective laser melting process: A comprehensive review. *J. Manuf. Syst.* **2022**, *63*, 250–274. [[CrossRef](#)]
2. Li, W.; Yu, G.; Yu, Z. Bioinspired heat exchangers based on triply periodic minimal surfaces for supercritical CO₂ cycles. *Appl. Therm. Eng.* **2020**, *179*, 115686. [[CrossRef](#)]
3. Thomas, N.; Sreedhar, N.; Al-Ketan, O.; Rowshan, R.; Abu Al-Rub, R.K.; Arafat, H. 3D printed triply periodic minimal surfaces as spacers for enhanced heat and mass transfer in membrane distillation. *Desalination* **2018**, *443*, 256–271. [[CrossRef](#)]
4. Sithamparam, M.; Lai, L.S.; Tay, W.H. Computational Fluid Dynamics Simulation for Carbon Dioxide Gas Transport through Polydimethylsiloxane Membrane with Gyroid Structure. In *Materials Today: Proceedings*; Elsevier: Amsterdam, The Netherlands, 2021; Volume 46, pp. 1922–1928. [[CrossRef](#)]
5. Kibsgaard, J.; Jackson, A.; Jaramillo, T.F. Mesoporous platinum nickel thin films with double gyroid morphology for the oxygen reduction reaction. *Nano Energy* **2016**, *29*, 243–248. [[CrossRef](#)]
6. Zhao, M.; Zhang, D.Z.; Liu, F.; Li, Z.H.; Ma, Z.B.; Ren, Z.H. Mechanical and energy absorption characteristics of additively manufactured functionally graded sheet lattice structures with minimal surfaces. *Int. J. Mech. Sci.* **2020**, *167*, 105262. [[CrossRef](#)]
7. Plocher, J.; Panesar, A. Review on design and structural optimisation in additive manufacturing: Towards next-generation lightweight structures. *Mater. Des.* **2019**, *183*, 108164. [[CrossRef](#)]

8. Wallat, L.; Altschuh, P.; Reder, M.; Nestler, B.; Poehler, F. Computational Design and Characterisation of Gyroid Structures with Different Gradient Functions for Porosity Adjustment. *Materials* **2022**, *15*, 3730. [CrossRef]
9. Cooper, D.; Thornby, J.; Blundell, N.; Henrys, R.; Williams, M.; Gibbons, G. Design and manufacture of high performance hollow engine valves by Additive Layer Manufacturing. *Mater. Des.* **2015**, *69*, 44–55. [CrossRef]
10. Heisel, C.; Caliot, C.; Chartier, T.; Chupin, S.; David, P.; Rochais, D. Digital design and 3D printing of innovative SiC architectures for high temperature volumetric solar receivers. *Sol. Energy Mater. Sol. Cells* **2021**, *232*, 111336. [CrossRef]
11. Ali, M.; Sari, R.K.; Sajjad, U.; Sultan, M.; Ali, H.M. Effect of annealing on microstructures and mechanical properties of PA-12 lattice structures proceeded by multi jet fusion technology. *Addit. Manuf.* **2021**, *47*, 102285. [CrossRef]
12. Park, S.-Y.; Kim, K.-S.; AlMangour, B.; Grzesiak, D.; Lee, K.-A. Effect of unit cell topology on the tensile loading responses of additive manufactured CoCrMo triply periodic minimal surface sheet lattices. *Mater. Des.* **2021**, *206*, 109778. [CrossRef]
13. Abou-Ali, A.M.; Al-Ketan, O.; Lee, D.-W.; Rowshan, R.; Abu Al-Rub, R.K. Mechanical behavior of polymeric selective laser sintered ligament and sheet based lattices of triply periodic minimal surface architectures. *Mater. Des.* **2020**, *196*, 109100. [CrossRef]
14. Jia, H.; Lei, H.; Wang, P.; Meng, J.; Li, C.; Zhou, H.; Zhang, X.; Fang, D. An experimental and numerical investigation of compressive response of designed Schwarz Primitive triply periodic minimal surface with non-uniform shell thickness. *Extrem. Mech. Lett.* **2020**, *37*, 100671. [CrossRef]
15. Novak, N.; Kytyr, D.; Rada, V.; Doktor, T.; Al-Ketan, O.; Rowshan, R.; Vesenjak, M.; Ren, Z. Compression behaviour of TPMS-filled stainless steel tubes. *Mater. Sci. Eng. A* **2022**, *852*, 143680. [CrossRef]
16. Li, X.; Xiao, L.; Song, W. Compressive behavior of selective laser melting printed Gyroid structures under dynamic loading. *Addit. Manuf.* **2021**, *46*, 102054. [CrossRef]
17. Mishra, A.K.; Chavan, H.; Kumar, A. Effect of Material Variation on the Uniaxial Compression Behavior of FDM Manufactured Polymeric TPMS Lattice Materials. In *Materials Today: Proceedings*; Elsevier: Amsterdam, The Netherlands, 2021; Volume 46, pp. 7752–7759. [CrossRef]
18. Lu, C.; Zhang, C.; Wen, P.; Chen, F. Mechanical behavior of Al-Si10-Mg gyroid surface with variable topological parameters fabricated via laser powder bed fusion. *J. Mater. Res. Technol.* **2021**, *15*, 5650–5661. [CrossRef]
19. Fan, X.; Tang, Q.; Feng, Q.; Ma, S.; Song, J.; Jin, M.; Guo, F.; Jin, P. Design, mechanical properties and energy absorption capability of graded-thickness triply periodic minimal surface structures fabricated by selective laser melting. *Int. J. Mech. Sci.* **2021**, *204*, 106586. [CrossRef]
20. Ma, Q.; Zhang, L.; Ding, J.; Qu, S.; Fu, J.; Zhou, M.; Fu, M.W.; Song, X.; Wang, M.Y. Elastically-isotropic open-cell minimal surface shell lattices with superior stiffness via variable thickness design. *Addit. Manuf.* **2021**, *47*, 102293. [CrossRef]
21. Sobhani, S.; Muhunthan, P.; Boigné, E.; Mohaddes, D.; Ihme, M. Experimental Feasibility of Tailored Porous Media Burners Enabled via Additive Manufacturing. In *Proceedings of the Combustion Institute*; Elsevier: Amsterdam, The Netherlands, 2021; Volume 38, pp. 6713–6722. [CrossRef]
22. Bai, L.; Xu, Y.; Chen, X.; Xin, L.; Zhang, J.; Li, K.; Sun, Y. Improved mechanical properties and energy absorption of Ti6Al4V laser powder bed fusion lattice structures using curving lattice struts. *Mater. Des.* **2021**, *211*, 110140. [CrossRef]
23. Gavazzoni, M.; Beretta, S.; Foletti, S. Response of an aluminium Schwarz triply periodic minimal surface lattice structure under constant amplitude and random fatigue. *Int. J. Fatigue* **2022**, *163*, 107020. [CrossRef]
24. Kaur, I.; Singh, P. Flow and thermal transport characteristics of Triply-Periodic Minimal Surface (TPMS)-based gyroid and Schwarz-P cellular materials. *Numer. Heat Transf. Part A Appl.* **2021**, *79*, 553–569. [CrossRef]
25. Yin, H.; Zheng, X.; Wen, G.; Zhang, C.; Wu, Z. Design optimization of a novel bio-inspired 3D porous structure for crashworthiness. *Compos. Struct.* **2020**, *255*, 112897. [CrossRef]
26. Pure Copper AM Structures. 3D System's 2020. *Met. Powder Rep.* **2021**, *76*, 211. [CrossRef]
27. Handler, E.; Sterling, A.; Pegues, J.; Ozdes, H.; Masoomi, M.; Shamsaei, N.; Thompson, S.M. Design and Process Considerations for Effective Additive Manufacturing of Heat Exchangers. In *2017 International Solid Freeform Fabrication Symposium*; University of Texas: Austin, TX, USA, 2017.
28. Vaneker, T.; Bernard, A.; Moroni, G.; Gibson, I.; Zhang, Y. Design for additive manufacturing: Framework and methodology. *CIRP Ann.* **2020**, *69*, 578–599. [CrossRef]
29. Padrao, D.; Magnini, M.; Paterson, J.; Schoofs, F.; Tuck, D.C.H.; Maskery, I. Investigating Gyroid and Primitive Lattice Structures for Additively Manufactured Heat Exchangers. Energy Authority. 2022. Available online: <https://www.gov.uk/government/organisations/uk-atomic-energy-authority> (accessed on 10 October 2022).
30. Tirell, V. Advantages of 3D-printing heat exchangers. *Heat Exch. World* **2019**, 46–48. Available online: <https://aidro.it/wp-content/uploads/2021/03/hxw-46-48-additive-manufac-1.pdf> (accessed on 10 October 2022).
31. ISO/ASTM 52900:2015; Additive Manufacturing—General Principles—Terminology. ISO/ASTM: Geneva, Switzerland, 2018. Available online: <https://www.iso.org/standard/69669.html> (accessed on 10 October 2022).
32. Chen, L.-Y.; Liang, S.-X.; Liu, Y.; Zhang, L.-C. Additive manufacturing of metallic lattice structures: Unconstrained design, accurate fabrication, fascinated performances, and challenges. *Mater. Sci. Eng. R Rep.* **2021**, *146*, 100648. [CrossRef]
33. Cramer, C.L.; Ionescu, E.; Graczyk-Zajac, M.; Nelson, A.T.; Katoh, Y.; Haslam, J.J.; Wondraczek, L.; Aguirre, T.G.; LeBlanc, S.; Wang, H.; et al. Additive manufacturing of ceramic materials for energy applications: Road map and opportunities. *J. Eur. Ceram. Soc.* **2022**, *42*, 3049–3088. [CrossRef]

34. Soo, A.; Ali, S.M.; Shon, H.K. 3D printing for membrane desalination: Challenges and future prospects. *Desalination* **2021**, *520*, 115366. [CrossRef]
35. McDonough, J. A perspective on the current and future roles of additive manufacturing in process engineering, with an emphasis on heat transfer. *Therm. Sci. Eng. Prog.* **2020**, *19*, 100594. [CrossRef]
36. Yuan, S.; Li, S.; Zhu, J.; Tang, Y. Additive manufacturing of polymeric composites from material processing to structural design. *Compos. Part B Eng.* **2021**, *219*, 108903. [CrossRef]
37. Yang, L.; Han, C.; Wu, H.; Hao, L.; Wei, Q.; Yan, C.; Shi, Y. Insights into unit cell size effect on mechanical responses and energy absorption capability of titanium graded porous structures manufactured by laser powder bed fusion. *J. Mech. Behav. Biomed. Mater.* **2020**, *109*, 103843. [CrossRef]
38. Benedetti, M.; du Plessis, A.; Ritchie, R.; Dallago, M.; Razavi, S.; Berto, F. Architected cellular materials: A review on their mechanical properties towards fatigue-tolerant design and fabrication. *Mater. Sci. Eng. R Rep.* **2021**, *144*, 100606. [CrossRef]
39. Tijjing, L.D.; Dizon, J.R.C.; Ibrahim, I.; Nisay, A.R.N.; Shon, H.K.; Advincula, R.C. 3D printing for membrane separation, desalination and water treatment. *Appl. Mater. Today* **2019**, *18*, 100486. [CrossRef]
40. Gao, J.-Y.; Chen, S.; Liu, T.-Y.; Ye, J.; Liu, J. Additive manufacture of low melting point metal porous materials: Capabilities, potential applications and challenges. *Mater. Today* **2021**, *49*, 201–230. [CrossRef]
41. Ali, M.; Sajjad, U.; Hussain, I.; Abbas, N.; Ali, H.M.; Yan, W.-M.; Wang, C.-C. On the assessment of the mechanical properties of additively manufactured lattice structures. *Eng. Anal. Bound. Elem.* **2022**, *142*, 93–116. [CrossRef]
42. Al-Ketan, O.; Abu Al-Rub, R.K. Multifunctional Mechanical Metamaterials Based on Triply Periodic Minimal Surface Lattices. *Adv. Eng. Mater.* **2019**, *21*, 1900524. [CrossRef]
43. Zhang, X.; Zhang, K.; Zhang, L.; Wang, W.; Li, Y.; He, R. Additive manufacturing of cellular ceramic structures: From structure to structure–function integration. *Mater. Des.* **2022**, *215*, 110470. [CrossRef]
44. Seharang, A.; Azman, A.H.; Abdullah, S. A review on integration of lightweight gradient lattice structures in additive manufacturing parts. *Adv. Mech. Eng.* **2020**, *12*, 1687814020916951. [CrossRef]
45. Dixit, T.; Nithiarasu, P.; Kumar, S. Numerical evaluation of additively manufactured lattice architectures for heat sink applications. *Int. J. Therm. Sci.* **2020**, *159*, 106607. [CrossRef]
46. Balakrishnan, H.K.; Doeven, E.H.; Merenda, A.; Dumée, L.F.; Guijt, R.M. 3D printing for the integration of porous materials into miniaturised fluidic devices: A review. *Anal. Chim. Acta* **2021**, *1185*, 338796. [CrossRef]
47. Kim, J.; Yoo, D.-J. 3D printed compact heat exchangers with mathematically defined core structures. *J. Comput. Des. Eng.* **2020**, *7*, 527–550. [CrossRef]
48. Dixit, T.; Al-Hajri, E.; Paul, M.C.; Nithiarasu, P.; Kumar, S. High performance, microarchitected, compact heat exchanger enabled by 3D printing. *Appl. Therm. Eng.* **2022**, *210*, 118339. [CrossRef]
49. Nasuta, D.M.; Halota, A.; Zhao, A.; Mzhen, M. Advanced Copper Heat Exchangers from Low-Cost Additive Manufacturing Techniques. In Proceedings of the 19th International Refrigeration and Air Conditioning Conference at Purdue, West Lafayette, IN, USA, 10–14 July 2022. Available online: <https://docs.lib.purdue.edu/iracc> (accessed on 10 October 2022).
50. Feng, J.; Fu, J.; Yao, X.; He, Y. Triply periodic minimal surface (TPMS) porous structures: From multi-scale design, precise additive manufacturing to multidisciplinary applications. *Int. J. Extrem. Manuf.* **2022**, *4*, 022001. [CrossRef]
51. Ding, J.; Zou, Q.; Qu, S.; Bartolo, P.; Song, X.; Wang, C.C. STL-free design and manufacturing paradigm for high-precision powder bed fusion. *CIRP Ann.* **2021**, *70*, 167–170. [CrossRef]
52. Vaissier, B.; Pernot, J.-P.; Chougrani, L.; Véron, P. Lightweight Mesh File Format Using Repetition Pattern Encoding for Additive Manufacturing. *Comput. Des.* **2020**, *129*, 102914. [CrossRef]
53. Qin, Y.; Qi, Q.; Scott, P.; Jiang, X. Status, comparison, and future of the representations of additive manufacturing data. *Comput. Aided Des.* **2019**, *111*, 44–64. [CrossRef]
54. Cheng, L.; Liu, J.; To, A.C. Concurrent lattice infill with feature evolution optimization for additive manufactured heat conduction design. *Struct. Multidiscip. Optim.* **2018**, *58*, 511–535. [CrossRef]
55. Ma, S.; Tang, Q.; Feng, Q.; Song, J.; Han, X.; Guo, F. Mechanical behaviours and mass transport properties of bone-mimicking scaffolds consisted of gyroid structures manufactured using selective laser melting. *J. Mech. Behav. Biomed. Mater.* **2019**, *93*, 158–169. [CrossRef]
56. Qureshi, Z.A.; Al-Omari, S.A.B.; Elnajjar, E.; Al-Ketan, O.; Abu Al-Rub, R. On the effect of porosity and functional grading of 3D printable triply periodic minimal surface (TPMS) based architected lattices embedded with a phase change material. *Int. J. Heat Mass Transf.* **2021**, *183*, 122111. [CrossRef]
57. Yun, S.; Lee, D.; Jang, D.S.; Lee, M.; Kim, Y. Numerical analysis on thermo-fluid–structural performance of graded lattice channels produced by metal additive manufacturing. *Appl. Therm. Eng.* **2021**, *193*, 117024. [CrossRef]
58. Kelly, J.; Finkenauer, L.; Roy, P.; Stolaroff, J.; Nguyen, D.; Ross, M.; Hoff, A.; Haslam, J. Binder jet additive manufacturing of ceramic heat exchangers for concentrating solar power applications with thermal energy storage in molten chlorides. *Addit. Manuf.* **2022**, *56*, 102937. [CrossRef]
59. Spear, D.G.; Lane, J.S.; Palazotto, A.N.; Kemnitz, R.A. Computational based investigation of lattice cell optimization under uniaxial compression load. *Results Mater.* **2022**, *13*, 100242. [CrossRef]
60. Abueidda, D.W.; Abu Al-Rub, R.K.; Dalaq, A.S.; Lee, D.-W.; Khan, K.A.; Jasiuk, I. Effective conductivities and elastic moduli of novel foams with triply periodic minimal surfaces. *Mech. Mater.* **2016**, *95*, 102–115. [CrossRef]

61. Liu, F.; Zhou, T.; Zhang, T.; Xie, H.; Tang, Y.; Zhang, P. Shell offset enhances mechanical and energy absorption properties of SLM-made lattices with controllable separated voids. *Mater. Des.* **2022**, *217*, 110630. [CrossRef]
62. Ibrahim, Y.; Li, Z.; Davies, C.; Maharaj, C.; Dear, J.; Hooper, P. Acoustic resonance testing of additive manufactured lattice structures. *Addit. Manuf.* **2018**, *24*, 566–576. [CrossRef]
63. Al-Ketan, O.; Abu Al-Rub, R.K.; Rowshan, R. Mechanical Properties of a New Type of Architected Interpenetrating Phase Composite Materials. *Adv. Mater. Technol.* **2017**, *2*, 1600235. [CrossRef]
64. Kelly, C.N.; Kahra, C.; Maier, H.J.; Gall, K. Processing, structure, and properties of additively manufactured titanium scaffolds with gyroid-sheet architecture. *Addit. Manuf.* **2021**, *41*, 101916. [CrossRef]
65. Ramos, H.; Santiago, R.; Soe, S.; Theobald, P.; Alves, M. Response of gyroid lattice structures to impact loads. *Int. J. Impact Eng.* **2022**, *164*, 104202. [CrossRef]
66. Liverani, E.; Fortunato, A. Stiffness prediction and deformation analysis of Cobalt-Chromium lattice structures: From periodic to functionally graded structures produced by additive manufacturing. *J. Manuf. Process.* **2021**, *68*, 104–114. [CrossRef]
67. Pirotais, M.; Saintier, N.; Brugger, C.; Conesa, V. Ti-6Al-4V Lattices Obtained by SLM: Characterisation of the Heterogeneous High Cycle Fatigue Behaviour of Thin Walls. In *Procedia Structural Integrity*; Elsevier: Amsterdam, The Netherlands, 2021; Volume 38, pp. 132–140. [CrossRef]
68. Blakey-Milner, B.; Gradl, P.; Snedden, G.; Brooks, M.; Pitot, J.; Lopez, E.; Leary, M.; Berto, F.; du Plessis, A. Metal additive manufacturing in aerospace: A review. *Mater. Des.* **2021**, *209*, 110008. [CrossRef]
69. Montemurro, M.; Refai, K.; Catapano, A. Thermal design of graded architected cellular materials through a CAD-compatible topology optimisation method. *Compos. Struct.* **2021**, *280*, 114862. [CrossRef]
70. Du Plessis, A.; Razavi, S.M.J.; Benedetti, M.; Murchio, S.; Leary, M.; Watson, M.; Bhate, D.; Berto, F. Properties and applications of additively manufactured metallic cellular materials: A review. *Prog. Mater. Sci.* **2022**, *125*, 100918. [CrossRef]
71. Zhang, Z.; Wang, X.; Yan, Y. A review of the state-of-the-art in electronic cooling. *e-Prime* **2021**, *1*, 100009. [CrossRef]
72. Groth, J.-H.; Anderson, C.; Magnini, M.; Tuck, C.; Clare, A. Five simple tools for stochastic lattice creation. *Addit. Manuf.* **2021**, *49*, 102488. [CrossRef]
73. Baroutaji, A.; Arjunan, A.; Ramadan, M.; Robinson, J.; Alaswad, A.; Abdelkareem, M.A.; Olabi, A.-G. Advancements and prospects of thermal management and waste heat recovery of PEMFC. *Int. J. Thermofluids* **2021**, *9*, 100064. [CrossRef]
74. Li, W.; Yu, Z. Heat exchangers for cooling supercritical carbon dioxide and heat transfer enhancement: A review and assessment. *Energy Rep.* **2021**, *7*, 4085–4105. [CrossRef]
75. Liu, T.; Mauter, M.S. Heat transfer innovations and their application in thermal desalination processes. *Joule* **2022**, *6*, 1199–1229. [CrossRef]
76. Caket, A.G.; Wang, C.; Nugroho, M.A.; Celik, H.; Mobedi, M. Recent studies on 3D lattice metal frame technique for enhancement of heat transfer: Discovering trends and reasons. *Renew. Sustain. Energy Rev.* **2022**, *167*, 112697. [CrossRef]
77. Thole, K.A.; Lynch, S.P.; Wildgoose, A.J. Review of Advances in Convective Heat Transfer Developed through Additive Manufacturing. In *Advances in Heat Transfer*; Academic Press: Cambridge, MA, USA, 2021; Volume 53, pp. 249–325. [CrossRef]
78. Kaur, I.; Singh, P. State-of-the-art in heat exchanger additive manufacturing. *Int. J. Heat Mass Transf.* **2021**, *178*, 121600. [CrossRef]
79. Dutkowski, K.; Kruzal, M. Experimental Investigation of the Apparent Thermal Conductivity of Microencapsulated Phase-Change-Material Slurry at the Phase-Transition Temperature. *Materials* **2021**, *14*, 4124. [CrossRef]
80. Dutkowski, K. Air–Water Two-Phase Frictional Pressure Drop in Minichannels. *Heat Transf. Eng.* **2010**, *31*, 321–330. [CrossRef]
81. Maskery, I.; Parry, L.; Padrão, D.; Hague, R.; Ashcroft, I. FLatt Pack: A research-focussed lattice design program. *Addit. Manuf.* **2021**, *49*, 102510. [CrossRef]
82. Clarke, D.A.; Dolamore, F.; Fee, C.J.; Galvosas, P.; Holland, D.J. Investigation of flow through triply periodic minimal surface-structured porous media using MRI and CFD. *Chem. Eng. Sci.* **2020**, *231*, 116264. [CrossRef]
83. Khalil, M.; Ali, M.I.H.; Khan, K.A.; Abu Al-Rub, R. Forced convection heat transfer in heat sinks with topologies based on triply periodic minimal surfaces. *Case Stud. Therm. Eng.* **2022**, *38*, 102313. [CrossRef]
84. Zhianmanesh, M.; Varmazyar, M.; Montazerian, H. Fluid Permeability of Graded Porosity Scaffolds Architected with Minimal Surfaces. *ACS Biomater. Sci. Eng.* **2019**, *5*, 1228–1237. [CrossRef] [PubMed]
85. Guerra, B.M.B. Unsteady Flow and Heat Transfer through Triply Periodic Minimal Surfaces. Master’s Thesis, Universidade de Lisboa, Lisboa, Portugal, 2020.
86. Fan, Z.; Gao, R.; Liu, S. A novel battery thermal management system based on P type triply periodic minimal surface. *Int. J. Heat Mass Transf.* **2022**, *194*, 123090. [CrossRef]
87. Genç, A.M.; Vatanserver, C.; Koçak, M.; Karadeniz, Z.H. Investigation of additively manufactured triply periodic minimal surfaces as an air-to-air heat exchanger. In Proceedings of the REHVA 14th HVAC Word Confngress, Rotterdam, The Netherlands, 22–25 May 2022. [CrossRef]
88. Vignoles, G.L.; Rochais, D.; Chupin, S. Computation of the conducto-radiative effective heat conductivity of porous media defined by Triply Periodic Minimal Surfaces. *Int. J. Therm. Sci.* **2020**, *159*, 106598. [CrossRef]
89. Peng, H.; Gao, F.; Hu, W. Modeling and characterization of triply periodic minimal surface heat exchangers with additive manufacturing. In Proceedings of the 2019 International Solid Freeform Fabrication Symposium, Austin, TX, USA, 12–14 August 2019; Available online: <https://www.researchgate.net/publication/340077269> (accessed on 10 October 2022).

90. Passos, A.G.P.; da Silva Chaves Ribeiro Pereira, J.M.; de Almeida Mendes, M.A.; da Silva, C.F.N.B.; de Almeida Mendes, M.A. Laminar Flow and Heat Transfer in Triply Periodic Minimal Surfaces Mechanical Engineering Examination Committee. 2019. Available online: https://webcache.googleusercontent.com/search?q=cache:li3-k_xrDr0J:https://fenix.tecnico.ulisboa.pt/downloadFile/1126295043836647/ExtendedAbstractAndrePassos.pdf&cd=2&hl=pl&ct=clnk&gl=pl (accessed on 10 October 2022).
91. Sreedhar, N.; Thomas, N.; Al-Ketan, O.; Rowshan, R.; Hernandez, H.; Abu Al-Rub, R.K.; Arafat, H.A. 3D printed feed spacers based on triply periodic minimal surfaces for flux enhancement and biofouling mitigation in RO and UF. *Desalination* **2018**, *425*, 12–21. [[CrossRef](#)]
92. Qureshi, Z.A.; Al-Omari, S.A.B.; Elnajjar, E.; Al-Ketan, O.; Abu Al-Rub, R. Nature-inspired triply periodic minimal surface-based structures in sheet and solid configurations for performance enhancement of a low-thermal-conductivity phase-change material for latent-heat thermal-energy-storage applications. *Int. J. Therm. Sci.* **2022**, *173*, 107361. [[CrossRef](#)]
93. Cheng, Z.; Li, X.; Xu, R.; Jiang, P. Investigations on porous media customized by triply periodic minimal surface: Heat transfer correlations and strength performance. *Int. Commun. Heat Mass Transf.* **2021**, *129*, 105713. [[CrossRef](#)]
94. Al-Ketan, O.; Abu Al-Rub, R.K. MSLattice: A free software for generating uniform and graded lattices based on triply periodic minimal surfaces. *Mater. Des. Process. Commun.* **2020**, *3*, e205. [[CrossRef](#)]
95. Hsieh, M.-T.; Valdevit, L. Minisurf—A minimal surface generator for finite element modeling and additive manufacturing. *Softw. Impacts* **2020**, *6*, 100026. [[CrossRef](#)]
96. Jones, A.; Leary, M.; Bateman, S.; Easton, M. TPMS Designer: A tool for generating and analyzing triply periodic minimal surfaces. *Softw. Impacts* **2021**, *10*, 100167. [[CrossRef](#)]
97. Sosnowski, M.; Krzywanski, J.; Gnatowska, R. Polyhedral Meshing as an Innovative Approach to Computational Domain Discretization of a Cyclone in a Fluidized Bed CLC Unit. In *E3S Web of Conferences*; EDP Sciences: Les Ulis, France, 2017; Volume 14, p. 01027. [[CrossRef](#)]
98. Vlahinos, M.; O'hara, R. Unlocking Advanced Heat Exchanger Design and Simulation with nTop Platform and ANSYS CFX. 2020. Available online: <https://revolutioninsimulation.org/unlocking-advanced-heat-exchanger-design-and-simulation-with-ntop-platform-and-ansys-cfx/> (accessed on 10 October 2022).
99. Hesselmann, F.; Scherenberg, N.; Bongartz, P.; Djeljadini, S.; Wessling, M.; Cornelissen, C.; Schmitz-Rode, T.; Steinseifer, U.; Jansen, S.V.; Arens, J. Structure-dependent gas transfer performance of 3D-membranes for artificial membrane lungs. *J. Membr. Sci.* **2021**, *634*, 119371. [[CrossRef](#)]
100. Maloney, K.J.; Fink, K.D.; Schaedler, T.A.; Kolodziejska, J.A.; Jacobsen, A.J.; Roper, C.S. Multifunctional heat exchangers derived from three-dimensional micro-lattice structures. *Int. J. Heat Mass Transf.* **2012**, *55*, 2486–2493. [[CrossRef](#)]
101. Yun, S.; Kwon, J.; Lee, D.; Shin, H.H.; Kim, Y. Heat transfer and stress characteristics of additive manufactured FCCZ lattice channel using thermal fluid-structure interaction model. *Int. J. Heat Mass Transf.* **2019**, *149*, 119187. [[CrossRef](#)]
102. Plant, R.D.; Saghier, M.Z. Numerical and experimental investigation of high concentration aqueous alumina nanofluids in a two and three channel heat exchanger. *Int. J. Thermofluids* **2020**, *9*, 100055. [[CrossRef](#)]
103. Thompson, S.M.; Aspin, Z.S.; Shamsaei, N.; Elwany, A.; Bian, L. Additive manufacturing of heat exchangers: A case study on a multi-layered Ti–6Al–4V oscillating heat pipe. *Addit. Manuf.* **2015**, *8*, 163–174. [[CrossRef](#)]
104. Iasiello, M.; Cunsolo, S.; Bianco, N.; Chiu, W.; Naso, V. Developing thermal flow in open-cell foams. *Int. J. Therm. Sci.* **2017**, *111*, 129–137. [[CrossRef](#)]
105. Pelanconi, M.; Zavattoni, S.; Cornolti, L.; Puragliesi, R.; Arrivabeni, E.; Ferrari, L.; Gianella, S.; Barbato, M.; Ortona, A. Application of Ceramic Lattice Structures to Design Compact, High Temperature Heat Exchangers: Material and Architecture Selection. *Materials* **2021**, *14*, 3225. [[CrossRef](#)] [[PubMed](#)]
106. Aider, Y.; Kaur, I.; Cho, H.; Singh, P. Periodic heat transfer characteristics of additively manufactured lattices. *Int. J. Heat Mass Transf.* **2022**, *189*, 122692. [[CrossRef](#)]
107. Butler, C.; Babu, S.; Lundy, R.; Meehan, R.O.; Punch, J.; Jeffers, N. Effects of processing parameters and heat treatment on thermal conductivity of additively manufactured AlSi10Mg by selective laser melting. *Mater. Charact.* **2021**, *173*, 110945. [[CrossRef](#)]
108. Lorenzon, A.; Vaglio, E.; Casarsa, L.; Sortino, M.; Totis, G.; Saragò, G.; Lendormy, E.; Raukola, J. Heat transfer and pressure loss performances for additively manufactured pin fin arrays in annular channels. *Appl. Therm. Eng.* **2022**, *202*, 117851. [[CrossRef](#)]
109. Anvari, A.; Yancheshme, A.A.; Kekre, K.M.; Ronen, A. State-of-the-art methods for overcoming temperature polarization in membrane distillation process: A review. *J. Membr. Sci.* **2020**, *616*, 118413. [[CrossRef](#)]
110. Mousa, M.H.; Miljkovic, N.; Nawaz, K. Review of heat transfer enhancement techniques for single phase flows. *Renew. Sustain. Energy Rev.* **2020**, *137*, 110566. [[CrossRef](#)]
111. Shahbazi, A.; Ashtiani, H.A.D.; Afshar, H.; Jafarkazemi, F. Optimization of the SMX static mixer types thermal and hydraulic performance by coupling CFD-Genetic Algorithm. *Int. Commun. Heat Mass Transf.* **2021**, *126*, 105388. [[CrossRef](#)]
112. Sélo, R.R.; Catchpole-Smith, S.; Maskery, L.; Ashcroft, I.; Tuck, C. On the thermal conductivity of AlSi10Mg and lattice structures made by laser powder bed fusion. *Addit. Manuf.* **2020**, *34*, 101214. [[CrossRef](#)]
113. Ali, D.; Sen, S. Finite element analysis of mechanical behavior, permeability and fluid induced wall shear stress of high porosity scaffolds with gyroid and lattice-based architectures. *J. Mech. Behav. Biomed. Mater.* **2017**, *75*, 262–270. [[CrossRef](#)]
114. Pulvirenti, B.; Celli, M.; Barletta, A. Flow and Convection in Metal Foams: A Survey and New CFD Results. *Fluids* **2020**, *5*, 155. [[CrossRef](#)]

115. Luo, J.-W.; Chen, L.; Min, T.; Shan, F.; Kang, Q.; Tao, W. Macroscopic transport properties of Gyroid structures based on pore-scale studies: Permeability, diffusivity and thermal conductivity. *Int. J. Heat Mass Transf.* **2019**, *146*, 118837. [[CrossRef](#)]
116. Attarzadeh, R.; Rovira, M.; Duwig, C. Design analysis of the “Schwartz D” based heat exchanger: A numerical study. *Int. J. Heat Mass Transf.* **2021**, *177*, 121415. [[CrossRef](#)]
117. Attarzadeh, R.; Attarzadeh-Niaki, S.-H.; Duwig, C. Multi-objective optimization of TPMS-based heat exchangers for low-temperature waste heat recovery. *Appl. Therm. Eng.* **2022**, *212*, 118448. [[CrossRef](#)]
118. Baobaid, N.; Ali, M.I.; Khan, K.A.; Abu Al-Rub, R.K. Fluid flow and heat transfer of porous TPMS architected heat sinks in free convection environment. *Case Stud. Therm. Eng.* **2022**, *33*, 101944. [[CrossRef](#)]
119. Iyer, J.; Moore, T.; Nguyen, D.; Roy, P.; Stolaroff, J. Heat transfer and pressure drop characteristics of heat exchangers based on triply periodic minimal and periodic nodal surfaces. *Appl. Therm. Eng.* **2022**, *209*, 118192. [[CrossRef](#)]
120. Grande, M.C. Asif, Novel TPMS Contactors Designed with Imprinted Porosity: Numerical Evaluation of Momentum and Energy Transport. *SSRN Electron. J.* **2022**, *2*, 1–25. [[CrossRef](#)]
121. Qureshi, Z.A.; Al-Omari, S.A.B.; Elnajjar, E.; Al-Ketan, O.; Abu Al-Rub, R. Using triply periodic minimal surfaces (TPMS)-based metal foams structures as skeleton for metal-foam-PCM composites for thermal energy storage and energy management applications. *Int. Commun. Heat Mass Transf.* **2021**, *124*, 105265. [[CrossRef](#)]
122. Qureshi, Z.A.; Elnajjar, E.; Al-Ketan, O.; Abu Al-Rub, R.; Al-Omari, S.B. Heat transfer performance of a finned metal foam-phase change material (FMF-PCM) system incorporating triply periodic minimal surfaces (TPMS). *Int. J. Heat Mass Transf.* **2021**, *170*, 121001. [[CrossRef](#)]
123. Qureshi, Z.A.; Al Omari, S.A.B.; Elnajjar, E.; Mahmoud, F.; Al-Ketan, O.; Abu Al-Rub, R. Thermal characterization of 3D-Printed lattices based on triply periodic minimal surfaces embedded with organic phase change material. *Case Stud. Therm. Eng.* **2021**, *27*, 101315. [[CrossRef](#)]
124. Hariss, M.; Gounni, A.; El Alami, M. A practical guide on numerical and experimental investigations of solid-liquid phase-change heat transfer using some heat transfer enhancement techniques: Case study in Morocco. *J. Energy Storage* **2022**, *52*, 105070. [[CrossRef](#)]
125. Raja, S.; Hamulczuk, D.; Carlsson, S.D. Exploring a New Energy-Efficient Way to Heat Water. Design of a Heat Exchanger for Laundry Machine Applications Produced Using Additive Manufacturing. Available online: <https://odr.chalmers.se/handle/20.500.12380/302189?mode=full> (accessed on 10 October 2022).
126. Gerstler, W.; Erno, D. Introduction of an additively manufactured multi-furcating hest exchanger. In Proceedings of the 2017 16th IEEE Intersociety Conference on Thermal and Thermomechanical Phenomena in Electronic Systems (ITherm), Orlando, FL, USA, 30 May–2 June 2017.
127. Reynolds, B.W. *Simulation of Flow and Heat Transfer in 3D Printable Triply Periodic Minimal Surface Heat Exchangers*; University of Canterbury: Christchurch, New Zealand, 2020.
128. Alteneiji, M.; Ali, M.I.H.; Khan, K.A.; Abu Al-Rub, R.K. Heat transfer effectiveness characteristics maps for additively manufactured TPMS compact heat exchangers. *Energy Storage Sav.* **2022**, *1*, 153–161. [[CrossRef](#)]
129. Li, W.; Li, W.; Yu, Z. Heat Transfer Enhancement of Water-Cooled Triply Periodic Minimal Surface Heat Exchangers. *Appl. Therm. Eng.* **2022**, *217*, 119198. [[CrossRef](#)]
130. Wadsö, I.; Holmqvist, S. Additively Manufactured Heat Exchangers. Master’s Thesis, Lund University, Stockholm, Sweden, 2020.